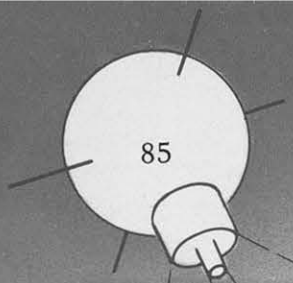

SATELLITE & MESOMETEOROLOGY RESEARCH PROJECT

Department of the Geophysical Sciences
The University of Chicago

MESOSCALE MODIFICATION OF SYNOPTIC SITUATIONS OVER THE AREA OF THUNDERSTORMS' DEVELOPMENT AS REVEALED BY ATS III AND AEROLOGICAL DATA

by

Kozo Ninomiya
The University of Chicago

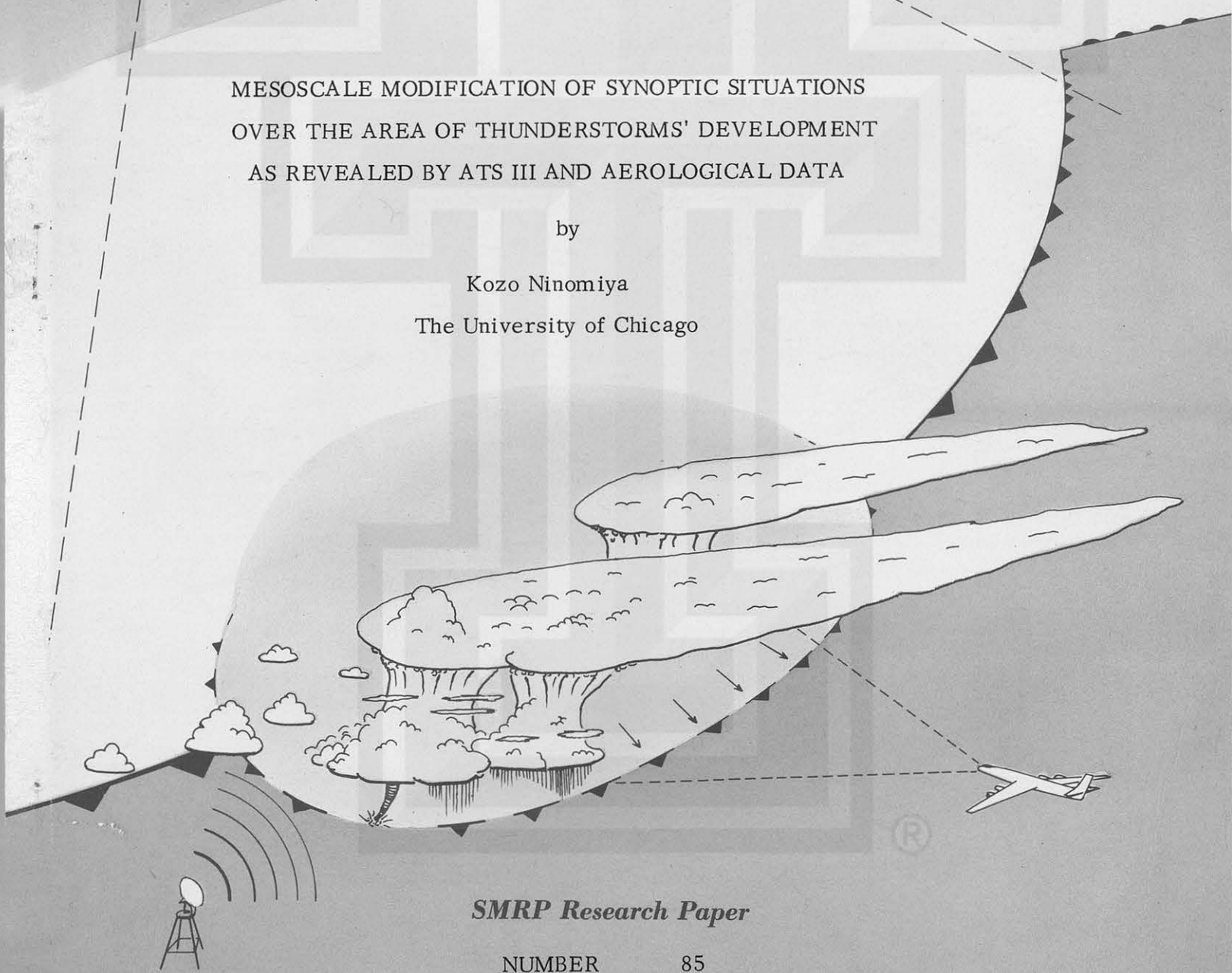

SMRP Research Paper

NUMBER 85

April 1970

MESOMETEOROLOGY PROJECT --- RESEARCH PAPERS

1.* Report on the Chicago Tornado of March 4, 1961 - Rodger A. Brown and Tetsuya Fujita

2.* Index to the NSSP Surface Network - Tetsuya Fujita

3.* Outline of a Technique for Precise Rectification of Satellite Cloud Photographs - Tetsuya Fujita

4.* Horizontal Structure of Mountain Winds - Henry A. Brown

5.* An Investigation of Developmental Processes of the Wake Depression Through Excess Pressure Analysis of Nocturnal Showers - Joseph L. Goldman

6.* Precipitation in the 1960 Flagstaff Mesometeorological Network - Kenneth A. Styber

7.** On a Method of Single- and Dual-Image Photogrammetry of Panoramic Aerial Photographs - Tetsuya Fujita

8. A Review of Researches on Analytical Mesometeorology - Tetsuya Fujita

9.* Meteorological Interpretations of Convective Nephsystems Appearing in TIROS Cloud Photographs - Tetsuya Fujita, Toshimitsu Ushijima, William A. Hass, and George T. Dellert, Jr.

10.* Study of the Development of Prefrontal Squall-Systems Using NSSP Network Data - Joseph L. Goldman

11. Analysis of Selected Aircraft Data from NSSP Operation, 1962 - Tetsuya Fujita

12. Study of a Long Condensation Trail Photographed by TIROS I - Toshimitsu Ushijima

13. A Technique for Precise Analysis of Satellite Data; Volume I - Photogrammetry (Published as MSL Report No. 14) - Tetsuya Fujita

14. Investigation of a Summer Jet Stream Using TIROS and Aerological Data - Kozo Ninomiya

15. Outline of a Theory and Examples for Precise Analysis of Satellite Radiation Data - Tetsuya Fujita

16. Preliminary Result of Analysis of the Cumulonimbus Cloud of April 21, 1961 - Tetsuya Fujita and James Arnold

17. A Technique for Precise Analysis of Satellite Photographs - Tetsuya Fujita

18.* Evaluation of Limb Darkening from TIROS III Radiation Data - S.H.H. Larsen, Tetsuya Fujita, and W.L. Fletcher

19. Synoptic Interpretation of TIROS III Measurements of Infrared Radiation - Finn Pedersen and Tetsuya Fujita

20.* TIROS III Measurements of Terrestrial Radiation and Reflected and Scattered Solar Radiation - S.H.H. Larsen, Tetsuya Fujita, and W.L. Fletcher

21. On the Low-level Structure of a Squall Line - Henry A. Brown

22.* Thunderstorms and the Low-level Jet - William D. Bonner

23.* The Mesoanalysis of an Organized Convective System - Henry A. Brown

24. Preliminary Radar and Photogrammetric Study of the Illinois Tornadoes of April 17 and 22, 1963 - Joseph L. Goldman and Tetsuya Fujita

25. Use of TIROS Pictures for Studies of the Internal Structure of Tropical Storms - Tetsuya Fujita with Rectified Pictures from TIROS I Orbit 125, R/O 128 - Toshimitsu Ushijima

26. An Experiment in the Determination of Geostrophic and Isallobaric Winds from NSSP Pressure Data - William Bonner

27. Proposed Mechanism of Hook Echo Formation - Tetsuya Fujita with a Preliminary Mesosynoptic Analysis of Tornado Cyclone Case of May 26, 1963 - Tetsuya Fujita and Robbi Stuhmer

28. The Decaying Stage of Hurricane Anna of July 1961 as Portrayed by TIROS Cloud Photographs and Infrared Radiation from the Top of the Storm - Tetsuya Fujita and James Arnold

29. A Technique for Precise Analysis of Satellite Data, Volume II - Radiation Analysis, Section 6. Fixed-Position Scanning - Tetsuya Fujita

30. Evaluation of Errors in the Graphical Rectification of Satellite Photographs - Tetsuya Fujita

31. Tables of Scan Nadir and Horizontal Angles - William D. Bonner

32. A Simplified Grid Technique for Determining Scan Lines Generated by the TIROS Scanning Radiometer - James E. Arnold

33. A Study of Cumulus Clouds over the Flagstaff Research Network with the Use of U-2 Photographs - Dorothy L. Bradbury and Tetsuya Fujita

34. The Scanning Printer and Its Application to Detailed Analysis of Satellite Radiation Data - Tetsuya Fujita

35. Synoptic Study of Cold Air Outbreak over the Mediterranean using Satellite Photographs and Radiation Data - Aasmund Rabbe and Tetsuya Fujita

36. Accurate Calibration of Doppler Winds for their use in the Computation of Mesoscale Wind Fields - Tetsuya Fujita

37. Proposed Operation of Intrumented Aircraft for Research on Moisture Fronts and Wake Depressions - Tetsuya Fujita and Dorothy L. Bradbury

38. Statistical and Kinematical Properties of the Low-level Jet Stream - William D. Bonner

39. The Illinois Tornadoes of 17 and 22 April 1963 - Joseph L. Goldman

40. Resolution of the Nimbus High Resolution Infrared Radiometer - Tetsuya Fujita and William R. Bandeen

41. On the Determination of the Exchange Coefficients in Convective Clouds - Rodger A. Brown

* Out of Print
** To be published

(Continued on back cover)

SATELLITE AND MESOMETEOROLOGY RESEARCH PROJECT

Department of the Geophysical Sciences

The University of Chicago

MESOSCALE MODIFICATION OF SYNOPTIC SITUATIONS OVER THE AREA OF THUNDERSTORMS' DEVELOPMENT AS REVEALED BY ATS III AND AEROLOGICAL DATA

by

K. Ninomiya

The University of Chicago

SMRP Research Paper No. 85

April 1970

The research reported in this paper has been supported by the Environmental Science Services Administration under Grant ESSA E-198-68-(G) and the National Severe Storms Laboratory under Grant USESSA E-22-41-69-(G).

MESOSCALE MODIFICATION OF SYNOPTIC SITUATIONS OVER THE AREA OF THUNDERSTORMS' DEVELOPMENT AS REVEALED BY ATS III AND AEROLOGICAL DATA[1]

by

Kozo Ninomiya[2]

The University of Chicago

ABSTRACT

Synoptical and dynamical aspects of the development of the tornado-producing thunderstorms of April 23, 1968, were studied by combining conventional observation data with ATS III pictures, with special emphasis on the interaction between the thunderstorms and large-scale field.

Results of the analysis revealed a significant modification of moisture, thermal and wind fields in the vicinity of the area where storms developed. The formations of the large-scale cloud band and moist tongue were due to the mesoscale convective disturbances that developed along the frontal zone. It was concluded that the formation of a mid-tropospheric warm core accompanied by a strong upper outflow was the result of a process of so-called convective warming.

Results of the analyses suggested that both the jet stream and the core of positive vorticity to the left of the jet stream were formed by the increased thermal gradient to the left of the warm core. It was inferred that the modified thermal field and vorticity field forced downward motion and produced the dry area to the rear of the storm area.

Another characteristic aspect brought out by the analyses was

---

[1]The research reported in this paper has been supported by the Environmental Science Services Administration under Grant ESSA E-198-68-(G) and the National Severe Storms Laboratory under Grant USESSA E-22-41-69-(G).

[2]On leave from the Meteorological Research Institute, Tokyo, Japan.

the intensification of a low-level jet stream. The downward convective transport of the horizontal momentum in the shear flow intensified the low-level jet. The low-level jet increased the convergence of the water-vapor flux ahead of the jet, thus maintaining the activity of thunderstorms.

1. Introduction

Synoptic conditions faborable for the development of severe local storms have been described by many authors. According to Fawbush, Miller, and Starret (1951) and Newton (1963 and 1967) these conditions can be summarized as follows: (1) potential convective instability, (2) availability of abundant moisture in the lower layer within a relatively narrow band (i.e., a moist tongue) with dry air aloft, (3) strong wind bands in the lower and upper levels and (4) some mechanism than can trigger the release of instability.

Although these situations are observed in most cases of severe storm development, the physical link whereby the large-scale conditions and the development of the mesoscale storm are related is still poorly understood. For example, the strong wind aloft over a storm area sometimes is considered to be a result of convective activities rather than the cause of storm development. Without special observational data, a precise discussion of such a mutual relation between large-scale and mesoscale phenomena would be difficult, because both the life time and the horizontal scale of the latter are so small compared to the frequency and the density of the conventional rawinsonde observations, respectively.

In the spring of 1968, NASA and ESSA conducted the Tornado Watch Experiment. On days when severe storms were expected, ATS III took pictures at 14-minute intervals. The tornado-producing thunderstorms of April 23, 1968, were selected as part of the experiment.

In this paper, a detailed synoptical and dynamical analyses on the development of the thunderstorms of April 23 will be made to clarify the physical interaction between large-scale phenomena and thunderstorms by using conventional rawinsonde data combined with ATS III pictures.

2. Synoptic Weather Situation of April 23rd

This section will be concerned with the synoptic situation of April 23, 1968. The surface, the 850-mb and the 500-mb weather maps at 0600 CST and 1800 CST on April 23, 1968, are shown in Fig. 1 and Fig. 2, respectively. As seen in Fig. 1 a moderately intense cyclone was situated over southwestern Wisconsin on the morning of April 23 and a cold front extended to the southwest of it. During the day, the cyclone moved slowly at 15 knots northeastward. While the cold front moved eastward, a secondary low-pressure center developed over eastern Michigan (see Fig. 2).

In the lower troposphere (see 850-mb maps in Figs. 1 and 2) there was a narrow zone of warm and moist air which was advected from the Gulf ahead of the cold front by a moderately strong southern air flow. There was a mid-tropospheric cut-off cold air mass to the east of the cyclone which initially severed from the main cold air-mass in the evening of April 22. While the main cold trough aloft moved very slowly, the cut-off cold core moved northeastward at 40 knots (see 500-mb maps in Figs. 1 and 2). As the cut-off cold core moved over the Great Lakes region, it passed over the moist tongue in the lower layer. Remarkably unstable stratification, therefore, occurred over Indiana and Kentucky in the early afternoon of April 23. The initial development of the thunderstorms took place before noon over Indiana and they grew rapidly as they moved northeastward at 50 knots.

Fig. 3 contains the ATS III pictures at 0908 CST, 1155 CST and 1605 CST, April 23. The cloud vortex accompanying the cyclone was located towards Lake Michigan. A large-scale cloud band was found over the moist tongue in the lower troposphere. The cloud systems of the thunderstorms, which were observed as the bright cloud masses over Indiana at 1155 CST, grew quickly into a large cloud mass in a few hours. At 1605 CST, a huge triangle-shaped cloud mass from the thunderstorms was located to the south of Lake Erie.

During the 12-hour period from 0600 CST to 1800 CST, April 23, the remarkable changes in the thermal - wind field took place in the vicinity of the storm area. There was a warming area at the 500-mb surface at 1800 CST over the storm area and concurrently the mid-tropospheric jet stream formed to the northwest of the storm area.

In the lower troposphere (see the 850-mb map in Fig. 2), there was a low-level jet in the storm area at 1800 CST.

A schematic summary of the general situation of the day is presented in Fig. 4. The movement of the cyclone and the cold front at the 850-mb surface, the movement of the cut-off cold core, and the movement of the thunderstorms are indicated. The position of the axes of the upper-tropospheric jet stream at 0600 CST and at 1800 CST April 23 are also indicated in Fig. 4. As can be seen, the wind field in the upper troposphere changed remarkably during the developing and mature stage of the thunderstorms (see also Fig. 18 in section 6).

In the following sections, we will discuss the detail of the characteristic aspects of the thermal - wind field mentioned above.

3. The Role of the Cut-off Cold Core in the Thunderstorms' Development

a. Thermal Structure and Movement of the Cut-off Cold Core

It is well known that the development of severe storms is usually accompanied by the approach of a predominant cold air-mass aloft of a cold trough or a cut-off cold vortex (Fawbush, Miller and Starrett, 1951). As observed in Figs. 1 and 2 in the previous section, the cut-off cold core at the 500-mb surface was rather weak. We can, however, recognize the cold core more clearly by analyzing the thermal field at the 450-mb surface. Shown in Fig. 5 are the winds and thermal fields at the 450-mb surface in the vicinity of the cold core at 0600 CST. Figure 5 also shows the 300-mb thermal field and the pressure at the tropopause. In Fig. 6 the 450-mb and the 300-mb thermal fields at 1800 CST are presented. As observed in these figures, the cold core was quite intense at 450-mb. Although both the horizontal and the vertical scales of this cold core are much smaller than those of the typical cut-off cold vortex as studied by Newton and Palmen (1963), both showed the characteristic thermal structure of the cut-off cold vortex, i.e., the warm air mass at 300 mb and the depression of the tropopause above the cold core (see Figs. 5 and 6). (For similar cases of small cold vortices, see Matsumoto and Ninomiya (1967).)

The movement of the cold core and the change of the minimum temperature in the core are to be noted next. At 1800 CST, April 22, the eastward elongation of the cold air mass in the main cold trough, i.e., the indication of the cut-off, occurred over west Kansas. The movement of the cold core can be traced by tracing the center of the minimum temperature at 450 mb and that of the maximum temperature at 300 mb as shown in Fig. 6. While the main cold trough moved very slowly, the cut-off cold core moved northeastward at 40 knots. The minimum temperature of the cold core at 450 mb increased from -33°C to -27°C during the 12-hour period from 0600 CST to 1800 CST, April 23. This rapid increase of the temperature of the cold core indicates its rather rapid degeneration.

b. Influence of the Cut-off Cold Core on the Thunderstorms' Development

One of the influences of the cold core upon the thunderstorms' development is the thermal one. The cold advection in front of the cold air mass aloft, or, in other words, the decrease of the mid-tropospheric air temperature due to the passage of the cold core, over the moist tongue in the lower troposphere is a destabilizing factor. On the 500-mb maps in Figs. 1 and 2 of section 2, the area in which the difference between the equivalent potential temperature at 500 mb and that at 850 mb, i.e., when $\Delta\theta_e = \theta_{e_{500\,mb}} - \theta_{e_{850\,mb}}$ is less than 2°K was indicated by the stippled area. There was the unstable stratification under the cold core. Indeed, there were intense thunderstorms over eastern Michigan under the cold core during the afternoon and the evening of April 23.

Another influence of the cold core upon the thunderstorms' development is the dynamical one. The dynamically forced large-scale upward motion in the vicinity of the cold core works as a trigger for the release of the convective instability in the moist tongue. The use of the ω -equation is adequate to treat the large-scale vertical motion. Since we study here the field of vertical motion prior to the developing stage of the thunderstorms, the effect of the released latent heat in the condensation process is not considered. The ω -equation for adiabatic motion is

$$\sigma \nabla^2 \omega + f^2 \frac{\partial^2 \omega}{\partial p^2} = f \frac{\partial}{\partial p} \left[V_g \cdot \nabla (\zeta_g + f) \right] + \nabla^2 (V_g \cdot \nabla \alpha) \qquad (1)$$

where ω is vertical velocity ($= \frac{dp}{dt}$), α specific volume of air, f coriolis parameter, V_g geostrophic wind velocity and ζ_g geostrophic vorticity. The static stability σ is defined as $-\alpha \frac{\partial \ln \theta}{\partial p}$ where θ is potential temperature. As it is the intention of this study to clarify the role of the cold core in the thunderstorms' development, it will be adequate to simplify the equation to clarify the discussion.

For the horizontal sinusoidal and vertical parabolic distribution of ω, i.e.,

$$\omega = \omega_a \cdot \sin(\frac{2\pi}{L} x) \cdot \sin(\frac{2\pi}{L} y) \cdot \left[1 - (\frac{2p}{p_0} - 1)^2 \right] \qquad (2)$$

(the constant ω_a indicates the maximum value of ω, L is wavelength and p_0 is the surface pressure), we have

$$-A^2 \omega = f \frac{\partial}{\partial p} \left[V_g \cdot \nabla (\zeta_g + f) \right] + \nabla^2 (V_g \cdot \nabla \alpha) \qquad (3)$$

where

$$A^2 = 2\sigma (\frac{2\pi}{L})^2 + f^2 \frac{8}{p_0^2} . \qquad (4)$$

Eq. (3) states the well-known relation that the ascent motion tends to occur in regions of an upward increase of cyclonic vorticity advection and near maxima of warm temperature advection. To discuss the combined effect of the terms in the right side of eq. (3), it is convenient to rewrite eq. (3) as

$$-A^2 \omega = f \frac{\partial V_g}{\partial p} \cdot \nabla (\zeta_g + f) + (\nabla^2 V_g) \cdot \nabla \alpha + 2 (\frac{\partial V_g}{\partial x} \cdot \nabla \frac{\partial \alpha}{\partial x} + \frac{\partial V_g}{\partial y} \cdot \nabla \frac{\partial \alpha}{\partial y}) \qquad (5)$$

where we used the relation $V_g \cdot \nabla(\nabla^2 \alpha) = -f V_g \cdot \nabla \frac{\partial \zeta_g}{\partial p}$. The magnitude of $f \frac{\partial V_g}{\partial p} \cdot \nabla(\zeta_g + f)$ is usually larger than the magnitude of the second and the third terms, which means that the value of the vertical motion is dependent mainly on the first term. There we have

$$-A^2 \omega \cong f \frac{\partial V_g}{\partial p} \cdot \nabla (\zeta_g + f). \tag{6}$$

Eq. (6) states that ascent motion tends to occur within the region where the thermal wind blows from the area of the larger vorticity toward the area of smaller vorticity and descent motion within the region where the thermal wind blows from the area of the smaller vorticity toward larger vorticity (Eliassen, 1964). Shown in Fig. 7 are the field of the absolute geostrophic vorticity $(\zeta_g + f)$ on the 500-mb surface and the thickness between the 400-mb and the 700-mb surface. The hatched areas in the figure indicate the region where $\left| (V_{g\,400\,mb} - V_{g\,700\,mb}) \cdot \nabla (\zeta_g + f)_{500\,mb} \right|$ is more than 2×10^{-9} sec.$^{-1}$ Since the wavelength L is about 2,000 km, the value mentioned above corresponds to the absolute value of vertical velocity of 3 mb hour^{-1}. As seen in Fig. 7 the large scale upward motion was to the southeast of the cut-off cold core, over Indiana, in the morning of April 23. The moist tongue in the lower layer extended from the south to southern Indiana. The most favorable conditions for the thunderstorms' development existed in this area and the severe storms did actually develop there during the afternoon and the evening later on in the day.

4. The Formation of the Moist Tongue

a. Synoptical Aspects of the Moisture Field

The existence of the narrow belt of the moist and warm air in the lower layer is considered as one of the necessary conditions for storm development. The moist and warm air from the air mass over the Gulf of Mexico had been advected ahead of the cold front by the southerly flow as seen in both the surface and the 850-mb maps (Figs. 1 and 2). The areas indicated by stipples are the moist areas at the surface and that

at the 850-mb surface exceed 8 gm kg^{-1} and 6 gm kg^{-1}. The growth of the moist tongue, i.e., the elongating moist zone, during the 12 hours can be seen by comparing the moist areas indicated by stipples at 0600 CST with those at 1800 CST on April 23.

As observed in other cases of storms development (Fulks, 1951, Fawbush and Miller, 1953, Beebe, 1958) a remarkable inversion layer existed in the lower troposphere during the day. The height of the lower boundary of the inversion was not higher than 2,000 m above the surface in the morning of the day. Bounded by the inversion, the moist air mass was limited to the lowermost layer. This did not mean, however, that the air was very dry everywhere above the inversion. There was a narrow moist zone at the 700-mb surface even prior to the storms' development. As seen in the ATS III picture presented in Fig. 3, there was a large-scale cloud zone over the moist zone. Looking at this large-scale cloud zone and the moist tongue at 700 mb, one gets the impression that they are the direct cause of the storms' development.

In order to clarify the role of the large-scale moist zone, quantitative aspects of water-vapor transport will be analyzed. The horizontal transport vector of the water-vapor $\mathbf{V}q$ at each standard pressure surface at 0600 CST and 1800 CST are presented in Fig. 8. At 0600 CST, the largest horizontal transport was at the surface and/or at 850 mb and the magnitude of transport at 700 mb was generally small while the magnitude of transport at 700 mb is as large as that at 850 mb within the storm area at 1800 CST. Shown in Fig. 9 are the vertical distribution of the horizontal convergence of the water-vapor flux $\nabla \cdot \mathbf{V}q$ calculated by using the rawinsonde data at BNA, LIT, JAN and MGM for 0600 CST and PIT, DIA, GSO and HTS for 1800 CST April 23. Prior to the development of the thunderstorms, the horizontal convergence of water-vapor flux was observed mainly in the lower layer below the 800-mb surface while then as the thunderstorms had developed the layer of convergence of water-vapor flux reached as high as 600 mb. The results of analyses indicate that the strong convergence of water-vapor flux in the lowermost layer is the essential condition for thunderstorms' development, because it provides the abundant water vapor and the potential convective instability in the storm area prior to the storms' development. However, this conclusion does not contradict the fact that the large-scale cloud band or the

moist tongue at 700 mb is a symptom or, at least, a simultaneous phenomena of thunderstorms' development. Their formations indicate enough storage of water-vapor and potential instability in the lower layer.

b. Mesoscale Structure of the Moist Tongue

From the analyses of convective clouds, Matsumoto, Ninomiya and Akiyama (1967) concluded that convective clouds are organized into a mesoscale pattern and that the mesoscale convergence seems to influence the activity of the convective clouds. By analysing the water-vapor budget in the area of convective clouds, Ninomiya (1968) showed that the moisture field and cloud distribution are governed by the mesoscale convergence in the lower atmosphere. The assumption that the mesoscale convergence governs the moisture field and cloud distribution will be verified by analysing the detailed structure of the large-scale moist tongue and the cloud zone.

The cross section through the moist tongue and that through the storm area for 1800 CST, April 23, presented in Fig. 10 show the mesoscale structure of the moisture field in the large-scale moist tongue. In the cross section, thick stipples and thin stipples indicate the moist layers in which the dew-point depression is less than 2°C and 5°C. Figure 10 shows that the moisture field is not uniform throughout the large-scale moist zone and the mesoscale moist areas form the large-scale moist tongue. Shown in Fig. 11 are the distribution of clouds obtained from the ATS picture and the distribution of mixing ratio at the 850-, 700-and 500-mb surface at 1800 CST. The assumption that the mesoscale moist areas formed the moist tongue can be supported by comparing the cloud distribution with the moisture field given in Fig. 11. While the moist air mass at the surface (see the surface map in Fig. 2) covered almost all the area of the warm sector of the cyclone as well as the Gulf area, the moist areas at the 850-and 700-mb surface were only in the limited area where there were mesoscale convective disturbances.

One of the examples of the influence of the convective clouds upon the moist tongue was found near the Gulf coast around the Mexican border. As seen in Figs. 10 and 11 there are no indications of the moist zone or cloud zone in the windward

of the convective disturbance around the Mexican border. Convective motions in the disturbance brought the moist air in the lower layer up to the 700-mb surface. The moist air mass at 700 mb which flowed from the disturbance formed the moist tongue. As the moist air from the convective disturbance was advected leeward, both the humidity and the mixing ratio decreased due to the mixing of the relatively dry air. The large-scale moist tongue, however, was reintensified when it passed over another convective disturbance. Since there were several convective disturbances along the frontal zone, the large scale moist tongue was formed and/or maintained along the frontal zone.

A further example of the influence of the mesoscale convective disturbance upon the moisture field was observed over the storm area to the south of Lake Erie (Figs. 10 and 11). The horizontal convergence in the storm area was calculated to be 6×10^{-5} sec^{-1} at 850 mb by using rawinsonde data at DAY, HTS and PIT. The strong horizontal convergence in the lower layer brought the moist air up to the 400-mb surface. (For an example of similar aspects of the moisture field in the vicinity of the convective disturbance, see Matsumoto (1968).)

5. Intensification of the Low-level Jet

The large value of the horizontal transport of water vapor in the moist tongue at 850 mb (Fig. 8) was due to both the high mixing ratio and the strong wind speed. Moderately strong southwesterly wind was expected to be ahead of the cold front, because the pressure gradient was moderately strong in the vicinity of the cold front in the lower troposphere (Figs. 1 and 2). The wind speed, however, was not uniform in the moist tongue as observed in the 850-mb map at 1800 CST (Fig. 2). At 850 mb the wind speed at HTS was as high as 50 knots.

Fig. 12 shows the wind field on the 4,000 ft. level at 1200 CST and 1800 CST. There was a remarkable core of strong wind on this level. Since the horizontal wind shear around the core was as large as 8×10^{-5} sec^{-1}, it can be regarded as a low-level jet stream. Fig. 13 shows the wind distribution in the vertical cross section along the jet axis and that normal to the jet axis at 1800 CST. In the figure thick and thin lines

are isotaches (in knots) and isolines of vertical wind shear $\frac{\partial V}{\partial p}$ (in $m \cdot sec^{-1} \cdot km^{-1}$). Although no distinct maximum of wind speed is observed in the vertical profile of the wind speed, very strong vertical wind shear was observed in the layer between the 2,000-ft and the 3,000-ft level. In the figure, the layer of the positive shear is indicated by thin stipples and the layer in which the shear exceeds 20 $m \cdot sec^{-1} \cdot km^{-1}$ by dense stipples. The maximum vertical wind shear was as strong as 30 $m \cdot sec^{-1} \cdot km^{-1}$. Since the layer between the 4,000-ft and the 5,000-ft level was characterized by the non-vertical shear, the height of the core of the low-level jet was, probably, 4,000 ft or 5,000 ft above the ground.

A word of explanation is necessary concerning the strong wind above 8,000 ft over DAY (Fig. 13). It is not considered to be a low-level jet stream but the lower extension of the core of a mid-tropospheric jet stream (see Fig. 14a in section 6).

The strong low-level jets often occur in the western part of the Middle West. The jets are characterized by a distinct maximum wind in the lower level, long duration and nocturnal intensification. It has been proposed that the orographic effect and the frictional stress in the boundary layer cause its formation (Wexler (1961) and Hoecker (1963)). Sometimes, however, the low-level jet develops in an area where the orographic effect is not expected. (For example, see Matsumoto, Fujita and Asai (1962) and Matsumoto, personal communication.[3])

As the low-level jet in the case described here did not occur in the western part of the Middle West, the mechanism of its formation should differ from that proposed by Wexler (1961).

A few hours prior to the thunderstorms' development, at 0600 CST, no significant core of strong wind in the lower layer was recognized in the moist zone. Comparison of the wind field and the distribution of cloud and radar echo (Fig. 12) shows that the axis of strong wind was situated near the center of the convective area. The vertical wind profile at HTS (see Figs. 13 and 14a) was characterized by an almost uniform wind speed in the convective layer and strong vertical shear under the convective layer. (For a

---

[3]Personal communication on the results of the dynamical analysis on the low-level jet associated with intense rainfall over western Japan of July, 1968.

similar case see, Matsumoto, Ninomiya and Akiyama (1967), and Matsumoto and Ninomiya (1969a).) The characteristic wind profile mentioned above suggests the vertical convective mixing of the horizontal momentum in the convective layer. The downdraft in the storm area brings down the larger horizontal momentum from the upper convective layer into the lower convective layer and the updraft brings up the smaller momentum from the lower layer into the upper layer. Thus, as a whole, convective motions in the shear flow tend to decrease the wind speed in the upper layer and to increase the wind speed in the lower convective layer. Therefore the strong wind is formed on the base of the convective layer in the area of intense convections.

The convective mixing of the horizontal momentum, however, can not explain completely the mechanism of the low-level jet formation because there is the difference between the wind direction in the middle troposphere (about 240°) and that in the lower layer (about 210°). It would be necessary to introduce a mechanism of the adjustment of the imbalance between the pre-existing pressure gradient and the convectively intensified wind velocity to understand fully the dynamical process of the low-level jet formation. At present, however, the mechanism can not be studied because both density and frequency of rawinsonde observations were not sufficient for the analysis.

The modified wind field in the lower convective layer creates a favorable situation for the successive development of convective motions by producing the convergence ahead of the core of the low-level jet. (See Newton (1963), Matsumoto and Ninomiya (1969a and b).) In this case, the strong convergence and strong convergence of water-vapor flux are formed ahead of the core of the strong wind (Figs. 8 and 13). The maximum value of the horizontal convergence in front of the core was as large as $7 \times 10^{-5} \text{sec}^{-1}$.

6. The Modification of the Large-scale Wind and Thermal Field by the Thunderstorms

a. Formation of a Jet Stream

When the thunderstorms develop there is usually a strong wind zone in the upper layer as well as in the lower layer (Newton 1967). In this case, also, as seen in the 500-mb map at 1800 CST (Fig. 2 in section 2), there was a strong wind zone in

the vicinity of the storm area.

At 1800 CST, the strongest 500-mb wind more than 120 knots was observed at DAY. This strong wind will be described using cross-section analysis. Shown in Fig. 14a is the vertical cross section normal to the axis of the strong wind zone (see Line I in Fig. 16) Stations HTS and PIT were located within the storm area, DAY and DIA outside the storm area. The cross section shows that there was a strong wind core in the relatively narrow area to the northwest of the storm area while there were only weak winds over the storm area and to the south of it. The jet stream was characterized by strong horizontal and vertical wind shear as well as by high wind speed. The cross section shows a core of the mid-tropospheric warm air in the storm area and the strong horizontal thermal gradient to the northwest outside of the warm core. The strong vertical wind shear of the jet stream can be linked to the strong thermal gradient through the relation given by the thermal wind equation. The geostrophic wind profile, calculated by using the geopotential height at DAY, HTS and PIT is shown in the left side of Fig. 14a, which coincides well with that of the observed wind at DAY. (It should be noted that the winds recorded at the 400-, 300-and 250-mb surfaces at DAY were 40, 60 and 65 knots, respectively, at 0600 CST).

In order to compare the wind field in the vicinity of the storm area with that in the windward region of the storm area, the vertical cross section along the 90° W meridian is presented in Fig. 14b (see line II in Fig. 16). The distance between the cross section in Fig. 14a and that in Fig. 14b is no more than 800 km. In spite of the rather small distance, there are distinct differences between the wind and thermal situations in the two cross sections. Neither the mid-tropospheric warm core nor the mid-tropospheric jet stream can be observed in the cross section along the 90° W meridian. The nature of the strong wind over LIT differs from the nature of the jet stream over DAY (Fig. 14a) because the former is related to the thermal gradient in the upper troposphere which is characteristic of the thermal field in the vicinity of a high-level jet stream. Cross-sectional analyses suggest that the intensification of the wind speed (or formation of a jet stream) to the northwest of the storm area is caused mainly by the middle-tropospheric warming occuring in the storm area.

b. Middle-tropospheric Warm Core in the Storm Area

The characteristic features of the thermal field in the vertical cross section (Fig. 14a) are a distinct middle-tropospheric warm core in the storm area and the strong thermal gradient to the northwest outside the warm core. This warm core can be seen as a warm area in the 500-mb map (Fig. 2).

In the cross section, a deep moist layer was observed in the storm area while a very dry layer was to the northwest of the storm area.

By using rawinsonde data at PIT, HTS, GSO and DIA, the mean horizontal divergence over the quadrangle enclosed by these situations was calculated. The vertical velocity was then also calculated by using the continuity equation. The vertical distribution of the horizontal divergence and the vertical velocity in the storm area are presented in Fig. 15. As is seen in Fig. 15, the vertical velocity in the warm core is as large as 20 mb·hour^{-1}.

Because the high humidity, strong upward motion and the active convective clouds were observed in the warming area, the warming can be considered as the convective warming due to the release of the latent heat in the condensation process. It should be noted that a few hours prior to the thunderstorms' development, at 0600 CST, no warm core was recognized in the middle troposphere.

In order to express the entire effect of the warming in the convective layer, we will analyze the thickness field rather than the thermal field at a certain isobaric surface. Fig. 16 shows the thickness field between the 700-mb and the 400-mb surface and also the observed vertical wind shear in the same layer at 1800 CST, April 23. As seen in the figure there was an area of notable thickness, i.e., the area of warming, over the storm area and strong vertical shear along the northwestern border of warming area. (For an analysis of similar warm cores of convective storms see Matsumoto and Ninomiya (1967).)

In the analyses of the development of a tropical storm Yanai (1961) showed that the rapid deepening of sea-level pressure began after the formation of the warm core situation. It might be questioned whether or not the pressure deepening did occur under the influence of the convective warming in the middle latitude. Although no low-pressure

center was found in the storm area, there was a secondary maximum of pressure fall under the mid-tropospheric warm core. The value of the pressure fall during the 12-hour period between 0600 CST and 1800 CST was 10 mb. Some part of this pressure fall, of course, was due to the approach of the main cyclone. From the comparison of the value of the pressure fall in the storm area with that outside the storm area, we infer that 4-5 mb of the pressure fall was due to the convective warming.

c. Upper Outflow from Thunderstorms

The wind field in the upper troposphere in the vicinity of the storm area will be analyzed. Shown in Figs. 17a and 17b are the velocity field of the high cloud movement obtained by using the series of ATS III pictures taken during the 42-minute periods between 0841 and 0923 CST and 1538 and 1619 CST. Fujita and Bradbury (1969) and Ninomiya (1970) showed that the velocity of high clouds in the vicinity of the storm area coincides well with the wind velocity in the layer between the 200-mb and the 300-mb surface. Therefore, it can be assumed that the high cloud velocity field in Fig. 17a and Fig. 17b indicate the upper-tropospheric wind field before and after the thunderstorms' development. The 250-mb wind velocity obtained by rawinsonde observations at 0600 CST and 1800 CST are also presented in Figs. 17a and 17b. (In Fig. 17b, the wind at 440-mb at DAY and 370-mb at BNA are presented because the wind observations were missed above these levels.) The stream lines and the jet axes are indicated in the figures by solid lines and thick broken lines.

The wind field in Fig. 17b shows the notable change as compared with the field several hours earlier (Fig. 17a). The striking feature in Fig. 17b was the formation of the jet stream to the northwest of the storm area and the formation of the upper outflow field over the storm area.

It was already pointed out that there was a zone of strong thermal gradient to the northwest of the warm core (see Fig. 16). The formation of the jet stream can be linked to the strong thermal gradient through the relation given by the thermal wind equation.

The upper outflow field over the storm area was characterized by both the strong difluence and the strong horizontal divergence. The difference between the wind

direction in the northwestern side of the storm area and the wind direction in the southern side of the storm area was as large as 70°. The magnitude of the horizontal divergence over the storm area was more than 7×10^{-5} sec^{-1}. The outflow was considered to result from the upward mass transport across the base of the outflow layer due to the intense convective motions (see Fig. 15).

The results of the analyses in this section suggest that the warm core, the strong wind to the northwest of the storm area and the upper outflow should be considered as the results of the intense convective activity rather than the cause of the storms' development. At least, these phenomena should be considered as the simultaneous phenomena associated with the development of the thunderstorms.

More quantitative analyses on the warm core and upper outflow will be necessary in order to understand the physical aspects of the storms' development and will be made in a separate paper (Ninomiya 1970).

7. Intensification of the Dry Front

One of the interesting features of the moisture field is the very dry area to the northwest of the thunderstorms. As analyzed by Sawyer (1955), Fujita (1958) and the staff members of the National Severe Storms Project, the U.S. Weather Bureau (1963), the horizontal gradient of the mixing ratio in the transitional zone between the storm area and the dry area is sometimes very strong and thus could really be described as a dry front.

Since the dry air mass covered the vast area in the rear of the cold front, there was a moderately strong gradient of mixing ratio of the water vapor in the transitional zone between the dry and moist air mass (the 850-mb map in Fig. 2). The gradient of the mixing ratio, however, was not uniform along the transitional zone. As seen on the 850-mb map (Fig. 2) and the cross section (Fig. 14a), there was the extremely strong gradient of the mixing ratio in the rather narrow area in the rear of the storm area. This boundary between the moist area in the storm area and the extremely dry area in the rear of the storm area was also recognized in the ATS picture at 1605 CST (Fig. 3)

as the clear-cut boundary between convective cloud area and the cloudless area.

The fact that neither the extremely dry area nor the strong dry front was observed prior to the thunderstorms' development (see the 850-mb map at 0600 CST in Fig. 1), suggests that they developed simultaneously.

In order to clarify the mechanism of the dry front's formation, the water-vapor budget in the transitional zone in the rear of the storm area will now be analyzed by using rawinsonde data at DAY, HTS, BNA and AHN at 1800 CST.

The continuity equation of water vapor is

$$\overline{\frac{\partial q}{\partial t}} + \overline{\mathbf{V}\cdot\nabla q} + \overline{\omega}\,\frac{\partial \overline{q}}{\partial p} = 0 \qquad (7)$$

where p is pressure, q, mixing ratio, $\mathbf{V}$ and ω are horizontal and vertical wind velocity respectively. The bar —— indicates the areal mean. Neither the term of the condensation nor the term of convective transfer is necessary in the equation, since there were few convective clouds in the area under consideration. The vertical distribution of the horizontal divergence evaluated by using rawinsonde data at DAY, HTS, BNA and AHN is presented in Fig. 15 of section 6. The vertical velocity is calculated by using the continuity equation.

The local time change of the mixing ratio $\overline{\frac{\partial q}{\partial t}}$ is not evaluated directly except at the surface because the time interval of the rawinsonde observation is too long. Therefore to evaluate $\overline{\frac{\partial q}{\partial t}}$ the time-space transformation technique for the steady state was used as

$$\overline{\frac{\partial q}{\partial t}} = -\mathbf{C}\cdot\nabla q = -C\,\frac{\partial q}{\partial s} \qquad (8)$$

where $\mathbf{C}$ and C are the velocity and speed of system, and s is the distance measured in the direction of the velocity.

The results of the evaluation of eq. (8) are summarized in Table 1.

Table 1: The Water Vapor Budget for the Passing of the Dry Front (unit in $gm \cdot kg^{-1} \cdot hour^{-1}$).

Layer	$\overline{V \cdot \nabla q}$	$\bar{\omega} \frac{\overline{\partial q}}{\partial p}$	$\overline{V \cdot \nabla q} + \bar{\omega} \frac{\overline{\partial q}}{\partial p}$	$\frac{\overline{\partial q}}{\partial t}$
400 — 500 mb	0.15	0.09	0.24	-0.15
500 — 700 mb	0.24	0.32	0.56	-0.45
700 — 850 mb	0.22	0.21	0.43	-0.62
850 — 1000 mb	0.31	0.05	0.36	-0.57

It should be noted that in the layer between the 500-mb and the 850-mb surface, the magnitude of the vertical advection of water vapor $\bar{\omega} \frac{\overline{\partial q}}{\partial p}$ almost equals that of the horizontal advection of the water vapor $\overline{V \cdot \nabla q}$. The magnitude of the three dimensional advection of the water vapor coincides well with the magnitude of the local time change $\frac{\partial q}{\partial t}$. The rapid decrease of the mixing ratio is not only a result of horizontal advection. The results shown in Table 1 indicate that the strong downward advection due to the downward motion in the rear of the storm contribute greatly to the formation of the dry area and/or the dry front.

The detail of the dry front formation is not analyzed, however, by using the rawinsonde data because the time interval of the rawinsonde observation is 12 hours. The detail of the dry front formation will now be analyzed by using surface observation data. Shown in Fig. 18 are the isochrone of the dry front passage, or the isochrone of the occurrence time of the maximum decrease of the dewpoint temperature observed by the surface observation stations. The isolines of the maximum dewpoint-temperature decrease in one hour are also presented in the figure. In order to compare the position of the dry front at the surface with that in a higher level and the cloud distribution, the mixing ratio at the 700-mb surface and the cloud distribution obtained from the ATS picture

for 1800 CST are shown in the left figure of Fig. 18.

Fig. 18 shows that the dry front and/or dry area intensifies in a few hours as the thunderstorms developed and the maximum intensification occurred between 1600 CST and 1800 CST during which the thunderstorms reached their mature stage. The results of the surface analysis suggest that the downward motion is not so strong prior to the development of the thunderstorms but intensifies rapidly when the storms reached their mature stage.

8. The Modification of the Vertical Motion by the Thunderstorms

a. Vertical Motion in the Vicinity of the Storm Area

It was pointed out in sections 5, 6, and 7 that the field of vertical motion and divergence changed rapidly, as well as the horizontal wind field, during the several hours in the vicinity of the storm area. The upward motion in the storm area and the downward motion in the rear of the storm area intensified simultaneously as the thunderstorms developed.

In this section, the mechanism of the intensification of vertical motion and the influence of the thunderstorms upon the vertical motion will be analyzed by means of the ω -equation. It should be noted that it is not this author's intent to analyse the vertical motion of each thunderstorm but the mean vertical motion in the whole storm area or the dry area. Since the horizontal scale of these areas is 500-1000 km, the use of the ω -equation would be rather adequate. The ω -equation for the diabatic motion is

$$\sigma \nabla^2 \omega + f^2 \frac{\partial^2 \omega}{\partial p^2} + \frac{R}{c_p} \frac{1}{p} \nabla^2 \left(\frac{\delta Q}{\delta t} \right) + \left\{ \nabla^2 \left[V \cdot \nabla \left(\frac{\partial \phi}{\partial p} \right) \right] - f \frac{\partial}{\partial p} \left[V \cdot \nabla (\zeta + f) \right] \right\} = 0 \tag{9}$$

where ϕ is the geopotential height, ζ , vorticity and f , coriolis parameter. The static stability σ is defined as $-\alpha \frac{\partial}{\partial p} \ln \theta$ where θ and α is potential temperature

and specific volume of the air, and $(\frac{\delta Q}{\delta t})$ is defined as diabatic heating.

The vertical motion caused by the third term and the last term is the thermally and dynamically forced vertical motion, respectively. In order to clarify the mechanism of the intensification of the vertical motion, the thermally and dynamically forced vertical motion will be analyzed separately in the following studies.

b. Influence of the Convective Warming upon the Upward Motion in the Storm Area

The thermal influence of the thunderstorms upon the upward motion is studied by using the ω -equation for thermally forced vertical motion.

$$\sigma \nabla^2 \omega + f^2 \frac{\partial^2 \omega}{\partial p^2} + \frac{R}{c_p} \frac{1}{p} \nabla^2 (\frac{\delta Q}{\delta t}) = 0 \quad . \tag{10}$$

In order to simplify eq. (10) we introduce the horizontal sinusoidal and vertical parabolic distribution of ω and $(\frac{\delta Q}{\delta t})$, i.e.,

$$\omega = \omega_a \cdot \sin(\frac{2\pi}{L} x) \cdot \sin(\frac{2\pi}{L} y) \cdot \left[1 - (\frac{2p}{p_0} - 1)^2\right] \tag{2}$$

and

$$(\frac{\delta Q}{\delta t}) = (\frac{\delta Q}{\delta t})_a \cdot \sin(\frac{2\pi}{L} x) \cdot \sin(\frac{2\pi}{L} y) \cdot \left[1 - (\frac{2p}{p_0} - 1)^2\right] \tag{11}$$

where p_0 is the surface pressure and L is the wavelength. The constant ω_a and $(\frac{\delta Q}{\delta t})_a$ indicate the maximum value of ω and $(\frac{\delta Q}{\delta t})$, respectively. Rewriting eq. (10) by using eqs. (2) and (11), we have

$$-A^2 \omega_a - \frac{R}{c_p} \frac{1}{p} B^2 (\frac{\delta Q}{\delta t})_a = 0 \tag{12}$$

or

$$\omega_a = -\frac{B^2}{A^2} \frac{R}{c_p} \frac{1}{p} (\frac{\delta Q}{\delta t})_a \tag{12'}$$

where

$$A^2 = 2\sigma\left(\frac{2\pi}{L}\right)^2 + f^2\left(\frac{8}{p_0^2}\right) \tag{4}$$

and

$$B^2 = 2\left(\frac{2\pi}{L}\right)^2. \tag{13}$$

The amount of the areal mean precipitation in the central part of the storm area was 2 mm·hour^{-1}. Provided that the amount of condensation was equal to the amount of precipitation, the value of $\frac{1}{c_p}\left(\frac{\delta Q}{\delta t}\right)_a$ is approximately 0.75 ·hour^{-1}. Since the diameter of the storm area was about 500 km, we assume that L is 1000 km. The value of σ and f is approximately 0.25 cm^3 gm^{-1} mb^{-1} and 10^{-4} sec^{-1}, respectively. By putting these values in eq. (12′), the value of ω_a is evaluated to be approximately 20 mb·hour^{-1}.

The result of analysis shows that strong upward motion was caused by the release of latent heat in the storm area.

c. Dynamical Influence of the Thunderstorms upon the Vertical Motion

In section 3, by simplifying ω -equation, we related the vertical motion to the vorticity advection due to the thermal wind as

$$-A^2\omega \cong f\frac{\partial V_g}{\partial p}\cdot\nabla(\zeta + f). \tag{6}$$

---

[4]Since 120 cal·hour^{-1} of the latent heat is released by the 2 mm·hour^{-1} of condensation, we have

$$\frac{c_p}{g}\int_0^{p_0}\frac{1}{c_p}\left(\frac{\delta Q}{\delta t}\right)dp = \frac{c_p}{g}\frac{1}{c_p}\left(\frac{\delta Q}{\delta t}\right)_a\int_0^{p_0}\left[1-\left(\frac{2p}{p_0}-1\right)^2\right]dp = 120 \text{ cal}\cdot\text{hour}^{-1}$$

and the value of $\frac{1}{c_p}\left(\frac{\delta Q}{\delta t}\right)_a$ is obtained.

The dynamical influence of the thunderstorms upon the mean vertical motion is studied by using eq. (6).

It was already pointed out that the convective warming in the storm area intensified the thermal gradient to the northwest of the storm area and the formation of the zone of strong wind and the strong vertical shear could be linked to the intensified thermal gradient (section 6). The vorticity field was, therefore, modified greatly as the thunderstorms developed.

Fig. 19 shows the field of relative vorticity at the 500-mb surface at 1800 CST. In the figure, the field of thickness of the layer between 400 mb and 700 mb is also presented. The strong cyclonic vorticity outside the storm area and the strong anticyclonic vorticity inside the storm area are due to the strong horizontal wind shear in the vicinity of the jet stream.

In the vicinity of the area of cyclonic vorticity, the magnitude of $\frac{\partial V_g}{\partial p} \cdot \nabla(\zeta + f)$ was quite large, because both the thermal gradient and vorticity gradient are quite strong. The downward and upward motion is, therefore, forced dynamically in the windward side and the leeside of the center of cyclonic vorticity (Eliassen, 1963). The value of $(V_{g_{400\,mb}} - V_{g_{700\,mb}}) \cdot \nabla(\zeta + f)_{500\,mb}$ is approximately $10 \times 10^{-9}\ sec^{-2}$, and L (wavelength) is assumed to be 1000 km. By using eq. (6), the magnitude of the vertical motion is evaluated to be approximately 5 $mb \cdot hour^{-1}$.

The dynamically forced downward motion in the windward side of the area of the cyclonic vorticity, i. e., the rear left of the storm area, intensified the dry area and dry front (see section 7).

Although there was the strong anticyclonic vorticity in the storm area, the magnitude of the dynamically forced vertical motion was small because the thermal gradient and the thermal wind were weak over the storm area and to the south of the storm area.

d. Feedback Mechanism in Thunderstorms' Development

The results of analysis in sections 8b and 8c show that the upward motion was intensified in the storm area and in the leeside of the area of cyclonic vorticity (i. e.,

front-left of the storm area) due to the dynamical and thermal influence of thunderstorms.

The intensified upward motion and/or convergence in the lower troposphere in the storm area as well as the convergence of water-vapor flux in ahead of the low-level jet (section 5) create a favorable situation for the successive development of convective motions in and ahead of the storm area. This feedback mechanism due to the interaction between the thunderstorms and the large-scale (or medium-scale) field is assumed to be important in the development of the severe storms.

A word is necessary concerning the production of the kinetic energy in the vicinity of the storm area. The ascending of the air mass in the warm core and the descending of the cold air mass in the rear of the storm area converts available potential energy into kinetic energy. The produced kinetic energy intensifies the jet stream and therefore intensifies the vertical motion and thunderstorms. It should be noted that the production of the kinetic energy is also due to the thunderstorms because both the vertical motion and the warm air result from the development of the thunderstorms.

9. Concluding Remarks

From the analysis of the rawinsonde data and the ATS III pictures of the 23rd of April-1968-tornado-producing thunderstorms, we are able to conclude the following about the interaction between the large-scale field and the thunderstorms.

(1) A cut-off cold vortex aloft was important to the thunderstorms' development. The cold vortex and the warm, moist air flow in the lower troposphere provided the potential convective instability prior to the storms' development.

(2) The dynamically forced large-scale upward motion to the southeast of the cold vortex triggered the release of instability.

(3) The moist air mass was mainly in the lower troposphere under the inversion layer. The strong convergence of the water-vapor flux in the lower layer provided the abundant moisture and the potential instability prior to the thunderstorms' development.

(4) The large-scale cloud zone and the large-scale moist tongue in the higher layer developed simultaneously as the thunderstorms developed. They were caused and/or maintained by the mesoscale convective disturbances along the frontal zone.

(5) As the thunderstorms developed, the low-level jet was intensified in the storm area. The characteristic wind profile indicates that it was due to the convective transfer of horizontal momentum.

(6) The low-level jet provided the favorable condition for the successive development of thunderstorms by producing the convergence of water-vapor flux ahead of the low-level jet.

(7) There was convective warming (i. e. , the warm core) in the deep layer of the middle troposphere when the thunderstorms reached the mature stage.

(8) There was a strong outflow in the upper troposphere over the warm core. The strong upward motion in the warm core and the upper outflow were caused thermally by the convective warming.

(9) The convective warming caused the intensification of the horizontal thermal gradient and thus caused the formation of a jet stream to the northwest of the warm core. Therefore, there was the strong cyclonic vorticity to the left of the jet and the strong anticyclonic vorticity to the right of the jet.

(10) The strong thermal wind and the strong gradient of the vorticity to the northwest of the storm area caused dynamically downward motion in the rear-left of the storm area and upward motion front-left of the storm area.

(11) The downward motion caused the decrease of mixing-ratio in the rear of the storm area and a strong gradient of the mixing ratio was formed between the dry area and the storm area and the dry front was intensified.

These conclusions about the interaction between the thunderstorms and the large-scale field are summarized in the schematic model of the severe storms' development as presented in Fig. 20.

REFERENCES

Beebe, R. G., 1958; Tornado proximity soundings. Bull. Amer. Meteor. Soc. 39, 195-201.

Eliassen, A., 1964; Motions of intermediate scale; fronts and cyclones. Advances in Earth Science, The M. I. T. Press, 111-138.

Fawbush, E. J., and R. C. Miller, 1953; A method for forecasting hailstone size at the earth's surface. Bull. Amer. Meteor. Soc. 34, 235-244.

_____, _____, and L. G. Starrett, 1951; An empirical method of forecasting tornado development. Bull. Amer. Meteor. Soc. 32, 1-9.

Fujita, T., 1958; Structure and movement of a dry front. Bull. Amer. Meteor. Soc. 39, 574-582.

_____, and D. L. Bradbury, 1969; Determination of mass outflow from a thunderstorm complex using ATS III pictures. Proc. 6th Conf. Severe Local Storms, Amer. Meteor. Soc., 38-43.

Fulks, J. R., 1951; The instability line. Compendium of Meteorology, Amer. Meteor. Soc. 647-652.

Hoecker, W. H., 1963; Three southerly low-level jet systems delineated by the Weather Bureau special pibal network of 1961. Mon. Wea. Rev. 91, 573-582.

Matsumoto, S., 1968; Smaller scale disturbances in the temperature field around a decaying typhoon with special emphasis on the severe precipitation. J. Meteor. Soc. Japan 46, 483-495.

_____, T. Fujita, and T. Asai, 1962; Qualitative and quantitative analyses of severe rain storm of June 1961. Tenki, Japan Meteor. Soc. 9, 213-221.

_____, and K. Ninomiya, 1967; On the mesoscale warm core above the condensation level related to convective activities under the influence of dome shaped cold air. J. Meteor. Soc. Japan 45, 306-314.

_____, and _____, 1969a; Dynamical aspects of the mesoscale disturbance and its relation to the convective activity. Proc. 6th Conf. Severe Local Storms, Amer. Meteor. Soc., 44-47.

_____, and _____, 1969b; On the role of convective momentum exchange in the mesoscale gravity wave. J. Meteor. Soc. Japan 47, 75-85.

_____, _____, and T. Akiyama, 1967; Cumulus activities in relation to the mesoscale convergence field. J. Meteor. Soc. Japan 45, 292-305.

Newton, C. W., 1963; Dynamics of severe convective storms, Meteor. Mono. 5, No. 27, 33-58.

_____, 1967; Severe convective storms. Advances in Geophysics, Vol. 12, Academic Press, 257-308.

_____, and E. Palmen, 1963; Kinematic and thermal properties of a large-amplitude wave in the westerlies. Tellus 15, 99-119.

Ninomiya, K., 1968; Cumulus group activity over the Japan Sea in wintertime in relation to the water vapor convergence in subcloud layer. J. Meteor. Soc. Japan 46, 373-388.

_____, 1969; Dynamical analysis of outflow from tornado-producing thunderstorms as revealed by ATS III pictures. SMRP Research Paper #81, University of Chicago.

Sawyer, J.S., 1955; The free atmosphere in the vicinity of fronts. Geophysical Memoir 12, No. 96.

U.S. Weather Bureau, Staff Members of the National Severe Storms Project, 1963; Environmental and thunderstorm structures as shown by National Severe Storms Project observations in the spring 1960 and 1961. Mon. Wea. Rev. 91, 271-292.

Wexler, H., 1961; A boundary layer interpretation of the low-level jet. Tellus 13, 369-378.

Yanai, M., 1961; A detailed analysis of typhoon formation. J. Meteor. Soc. Japan 39, 187-214.

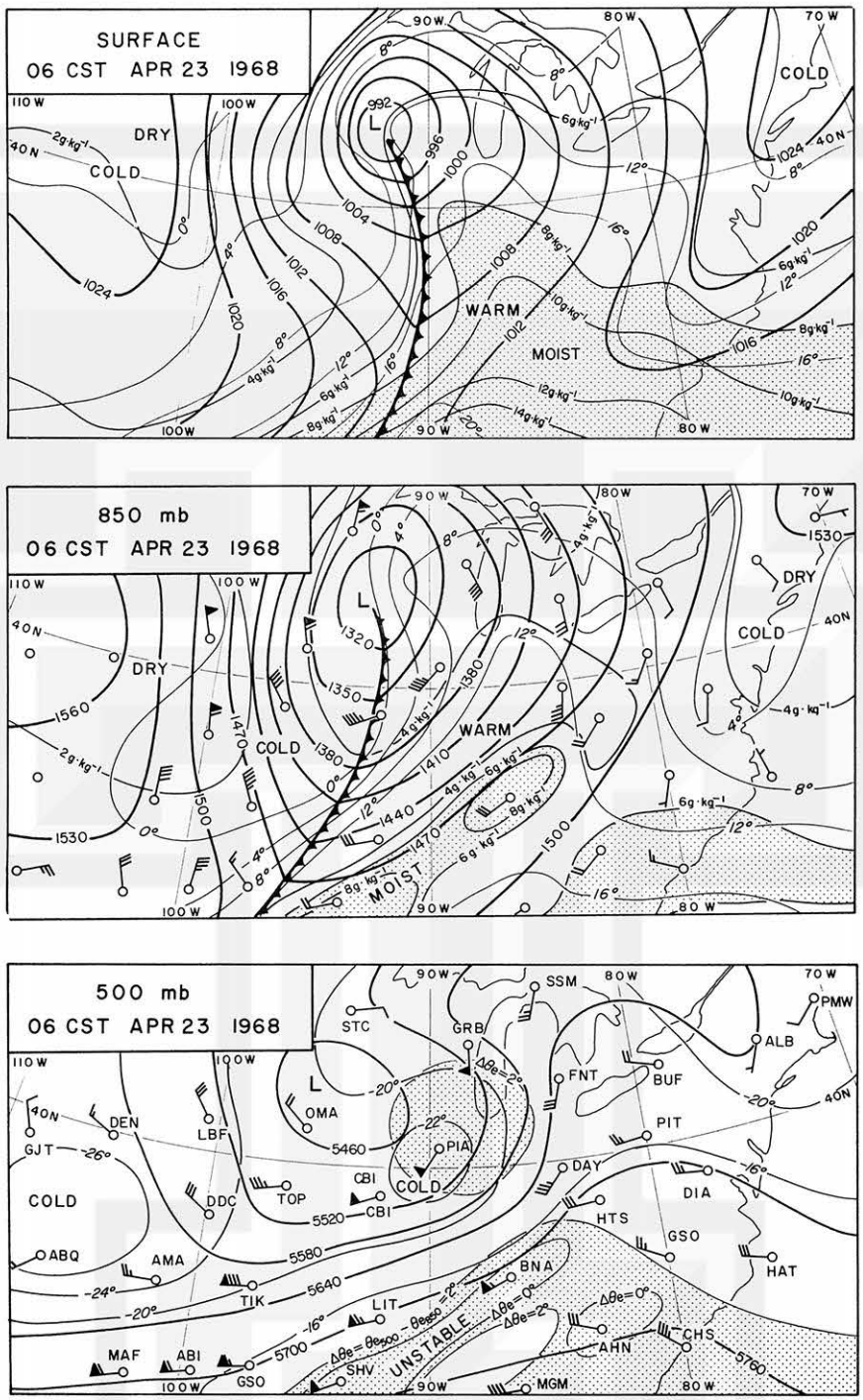

Fig. 1. Surface, 850-mb and 500-mb map at 0600 CST April 23, 1968. Isobars or contours and isotherms are indicated by thick and thin lines. The moist areas on the surface and the 850-mb map are indicated by stippling. On the 500-mb map, the area in which the difference between the equivalent potential temperature at 500 mb and that at 850 mb was less than 2°K are indicated by stippling.

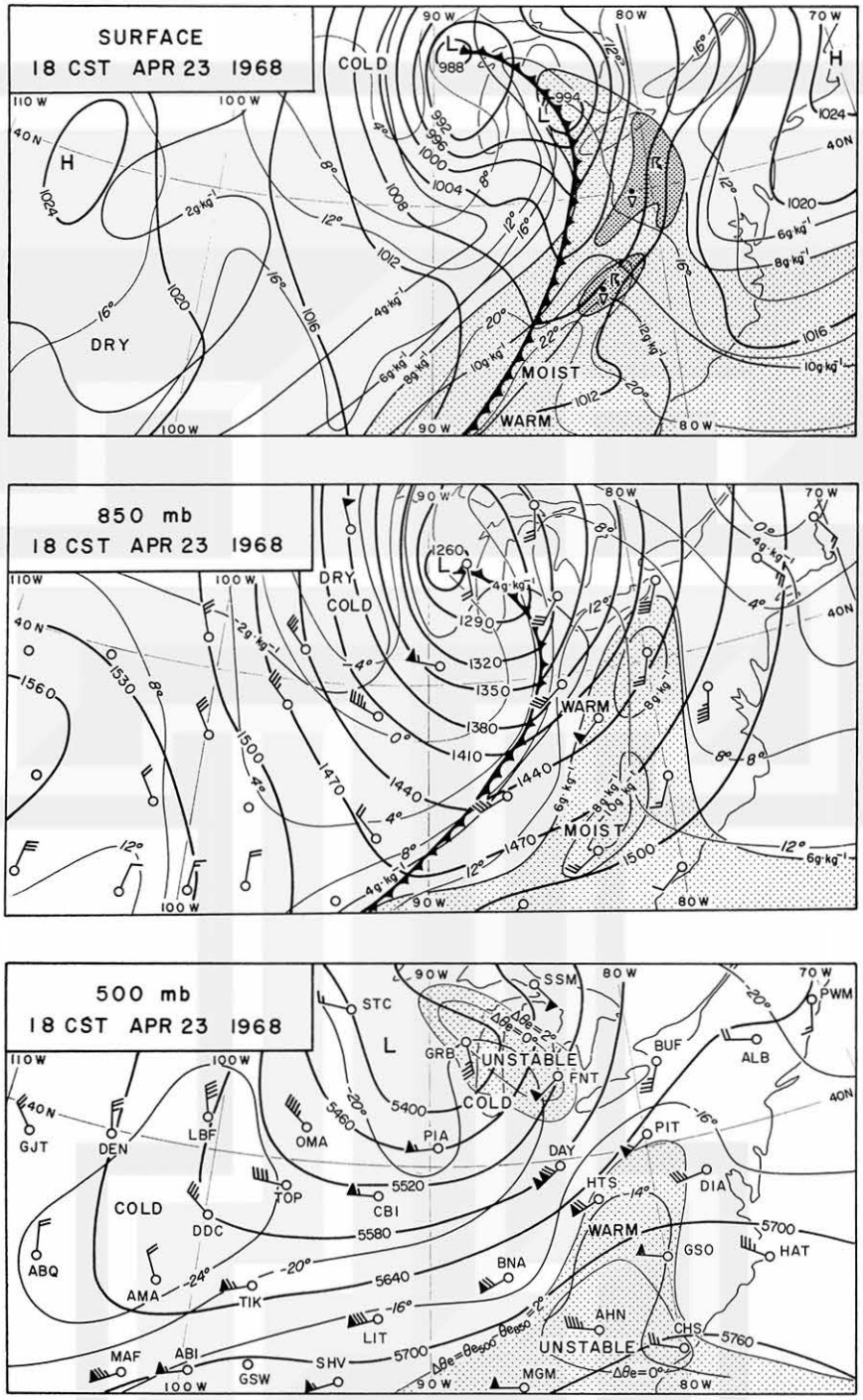

Fig. 2. Surface, 850-mb and 500-mb maps at 1800 CST, April 23, 1968.

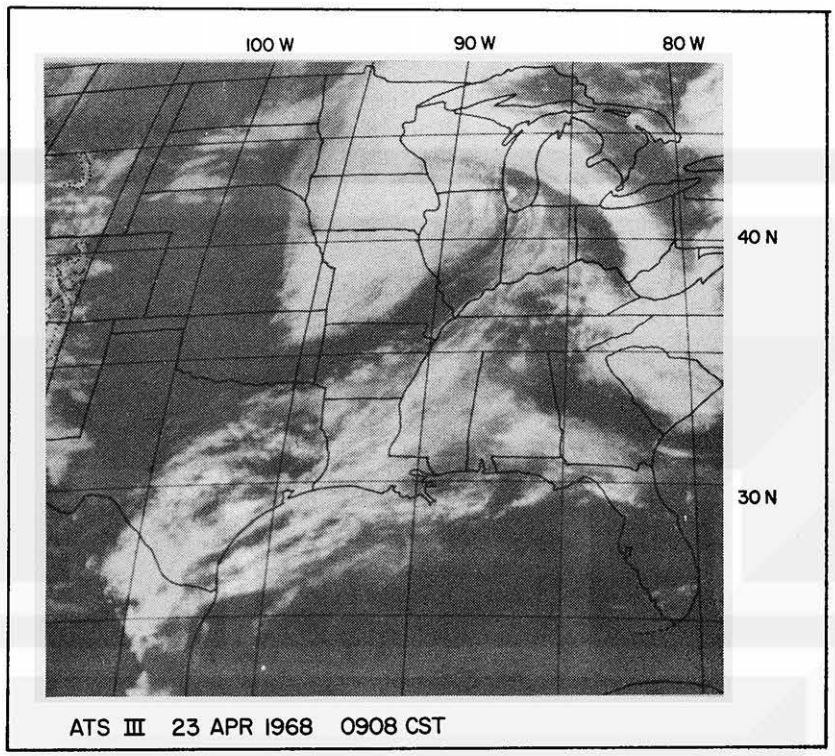

Fig. 3a. ATS III picture at 0908 CST.

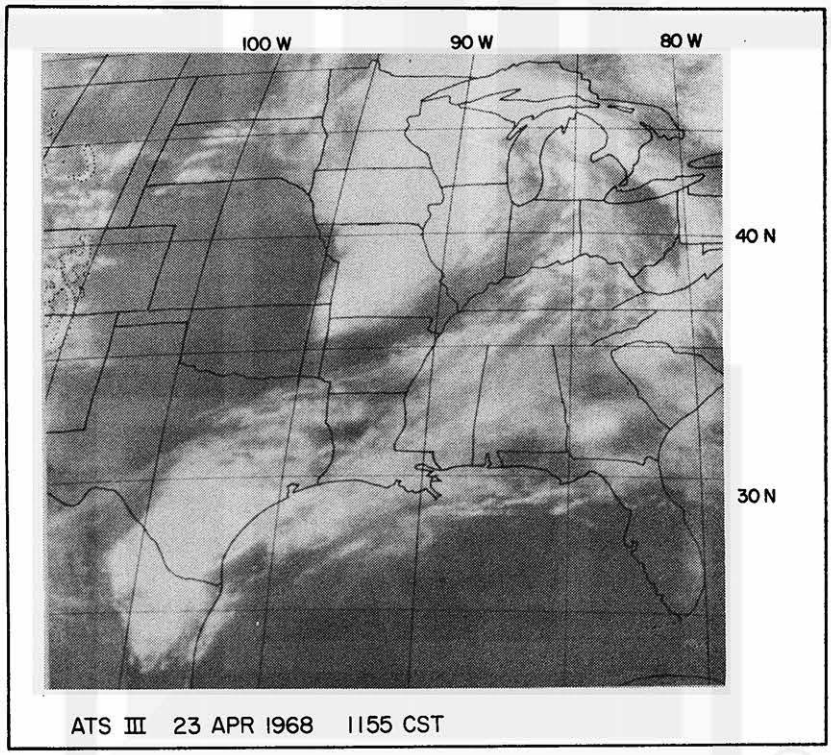

Fig. 3b. ATS III picture at 1155 CST.

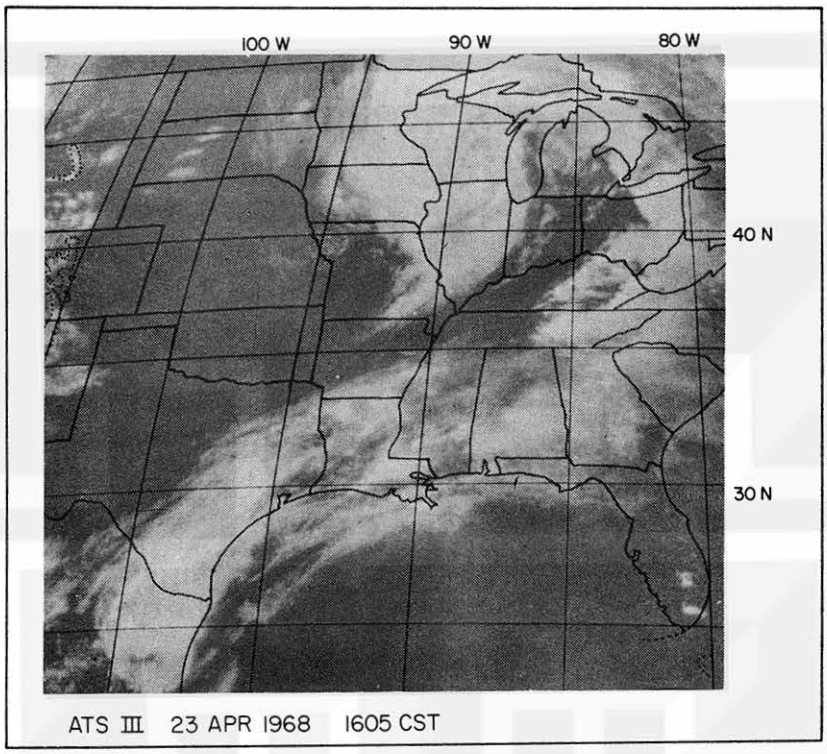

Fig. 3c. ATS III picture at 1605 CST.

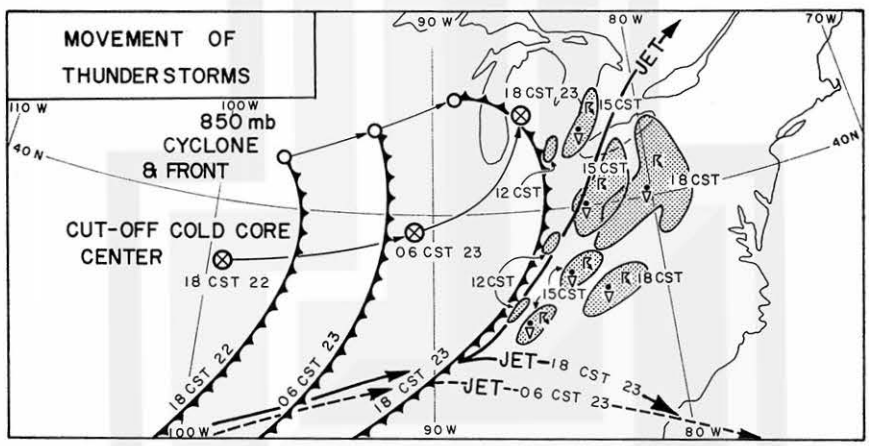

Fig. 4. Movement of the storm area, the cold front and the cut-off cold core.

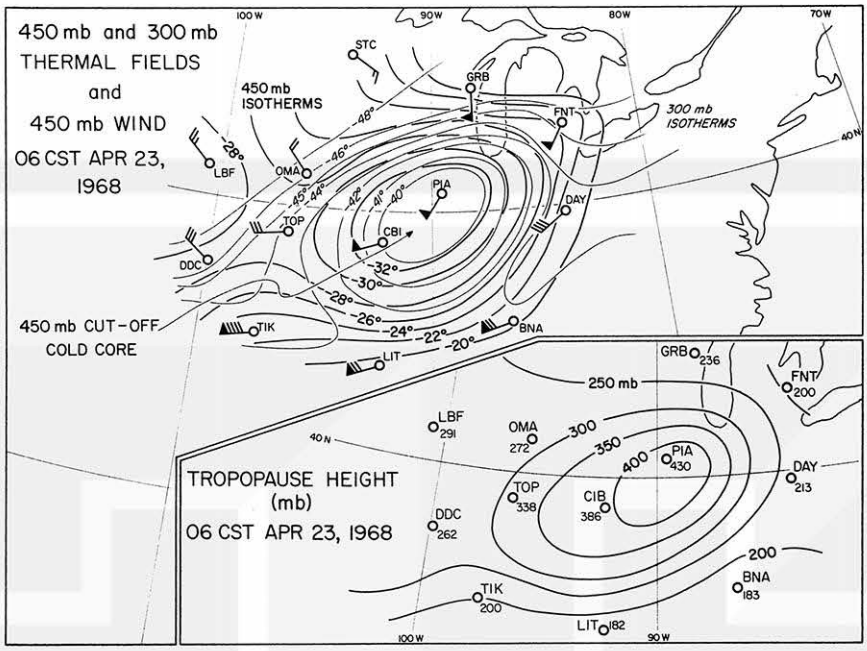

Fig. 5. Thermal field in the vicinity of the cut-off cold core at 0600 CST April 23.

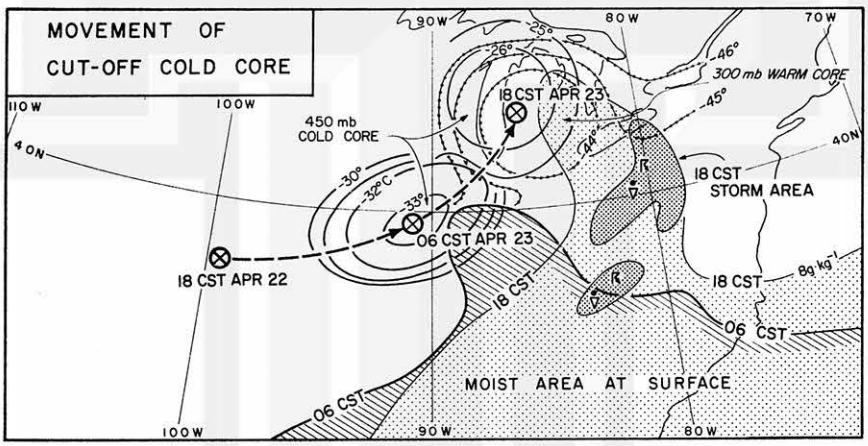

Fig. 6. Thermal field of the cold core at 1800 CST and the movement of the cold core.

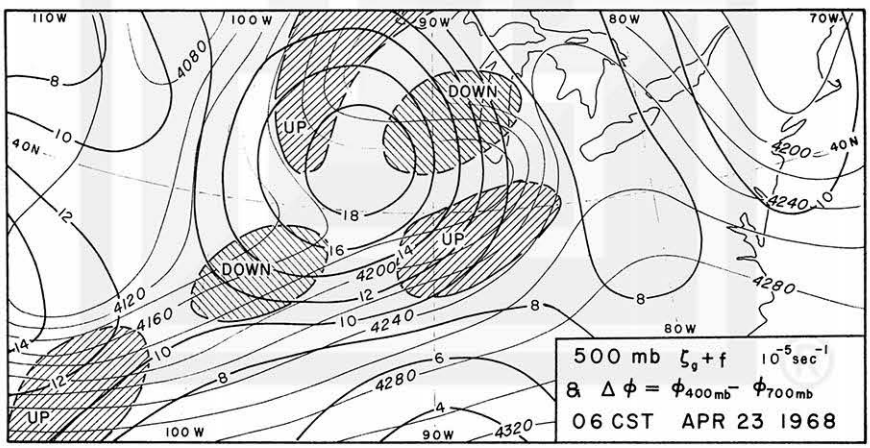

Fig. 7. Absolute geostrophic vorticity at the 500-mb surface and the thickness between the 400-mb and the 700-mb surfaces at 0600 CST.

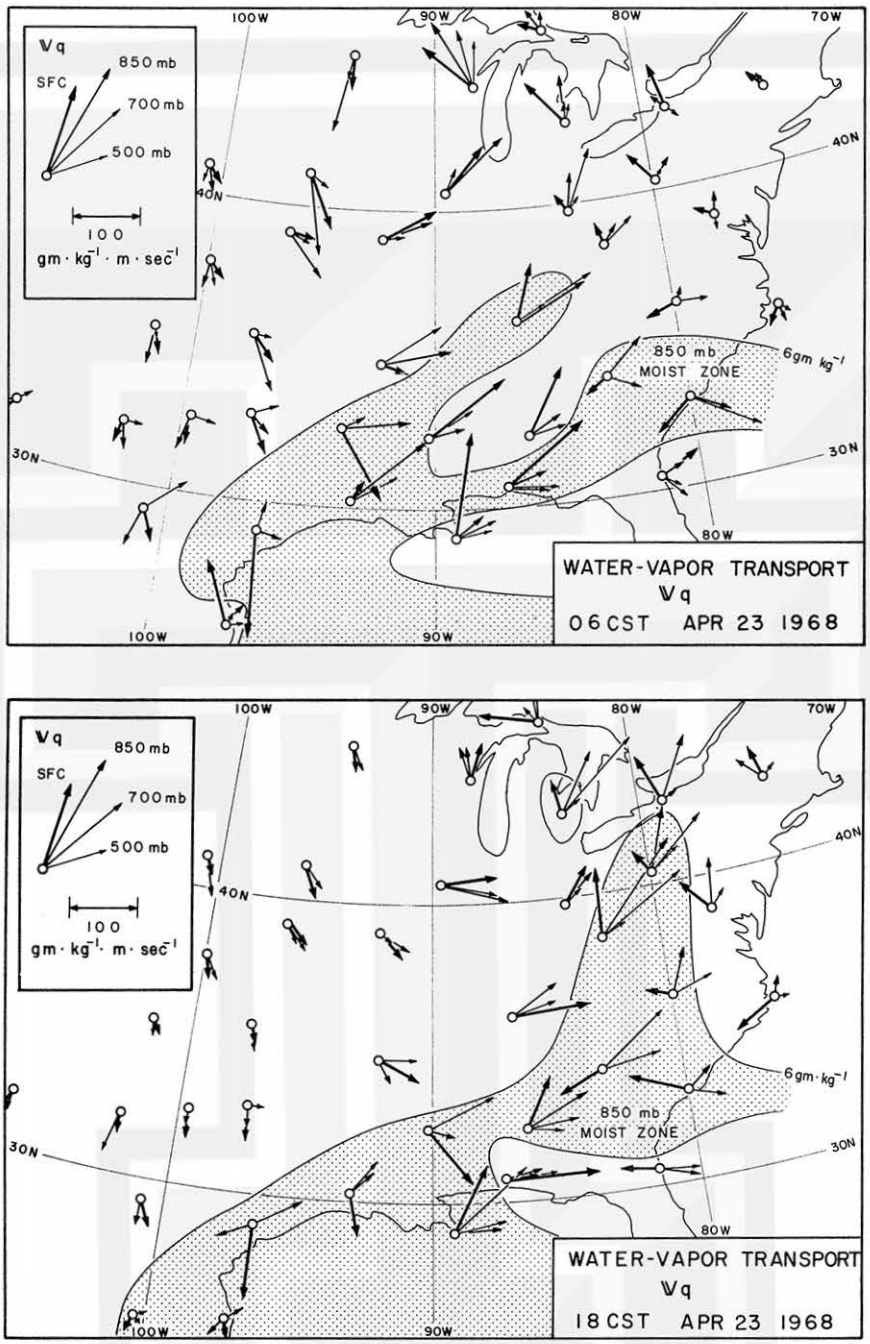

Fig. 8. Water-vapor transport at the surface, 850-mb, 700-mb and 500-mb surface at 0600 CST and 1800 CST.

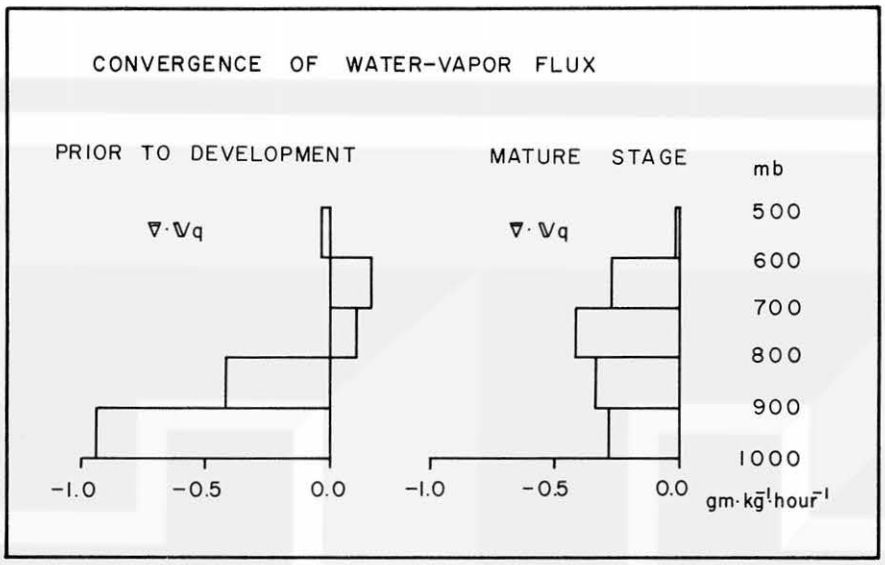

Fig. 9. Vertical distribution of the horizontal convergence of water vapor flux prior to the development of the storms and that in the mature stage of the storms.

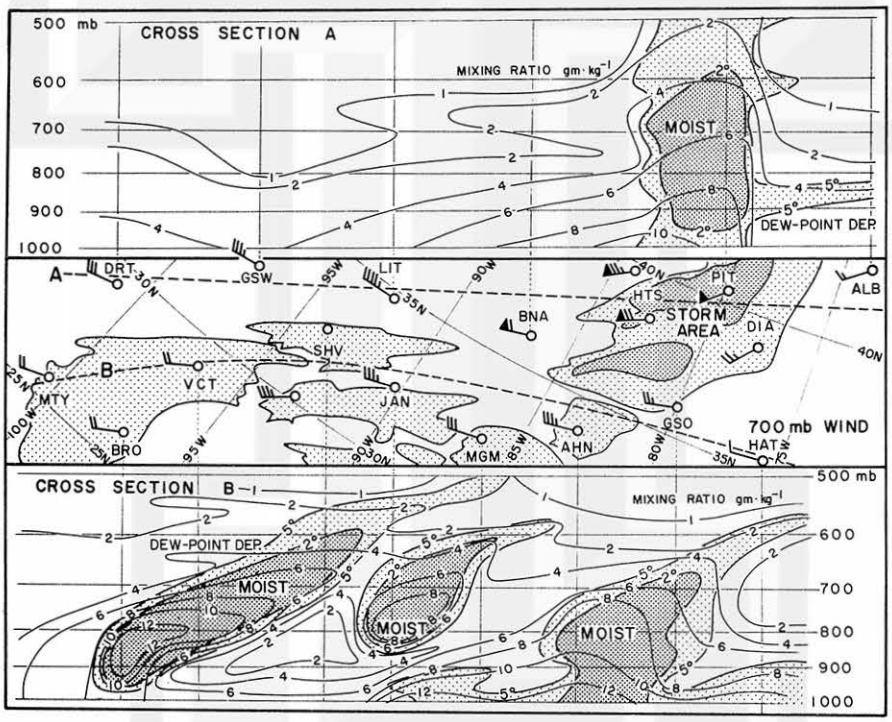

Fig. 10. Radar echo, cloud and the 700-mb wind in the moist tongue and the storm area and vertical cross sections through the moist tongue at 1800 CST. In the cross sections, isolines of the mixing ratio and the dewpoint depression are indicated by solid and thin lines.

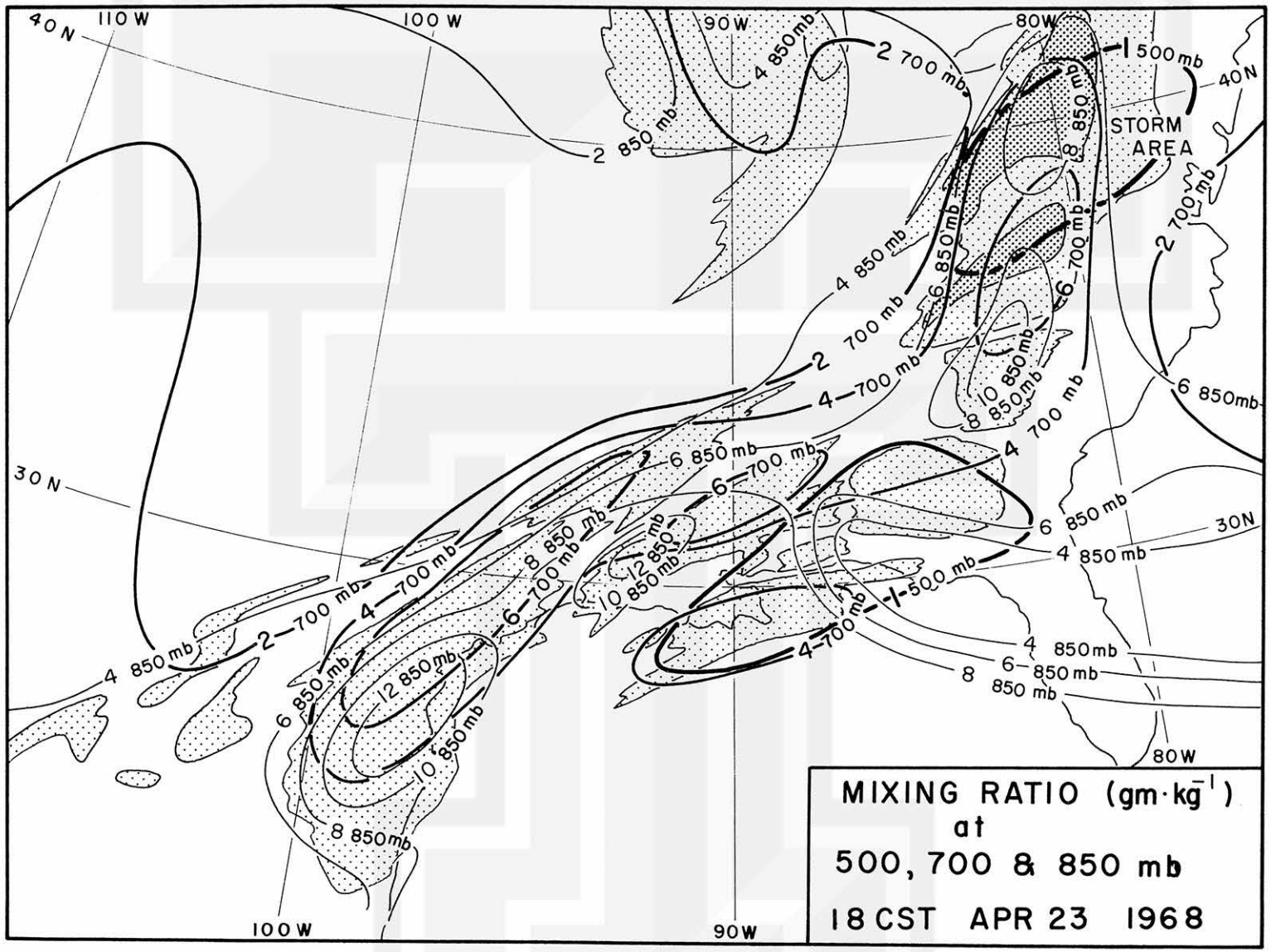

Fig. 11. Mixing ratio at the 850-mb, 700-mb and 500-mb surfaces, and cloud and radar echo at 1800 CST.

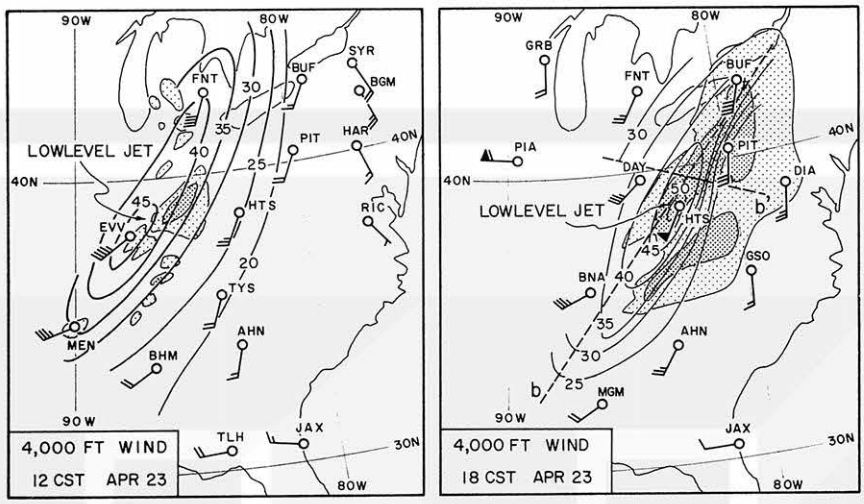

Fig. 12. The low-level jet stream on the 4,000 ft level, cloud and radar echo at 1200 CST and 1800 CST.

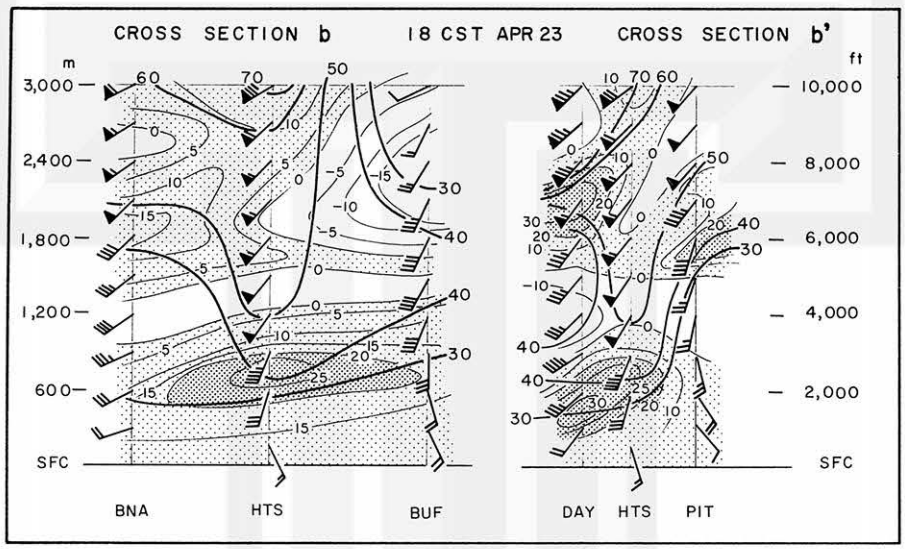

Fig. 13. The vertical cross section along and normal to the low-level jet at 1800 CST. Isotaches (knot) and isolines of vertical wind shear $\partial V/\partial Z$ (m sec^{-1} km^{-1}) are indicated by thick and thin lines.

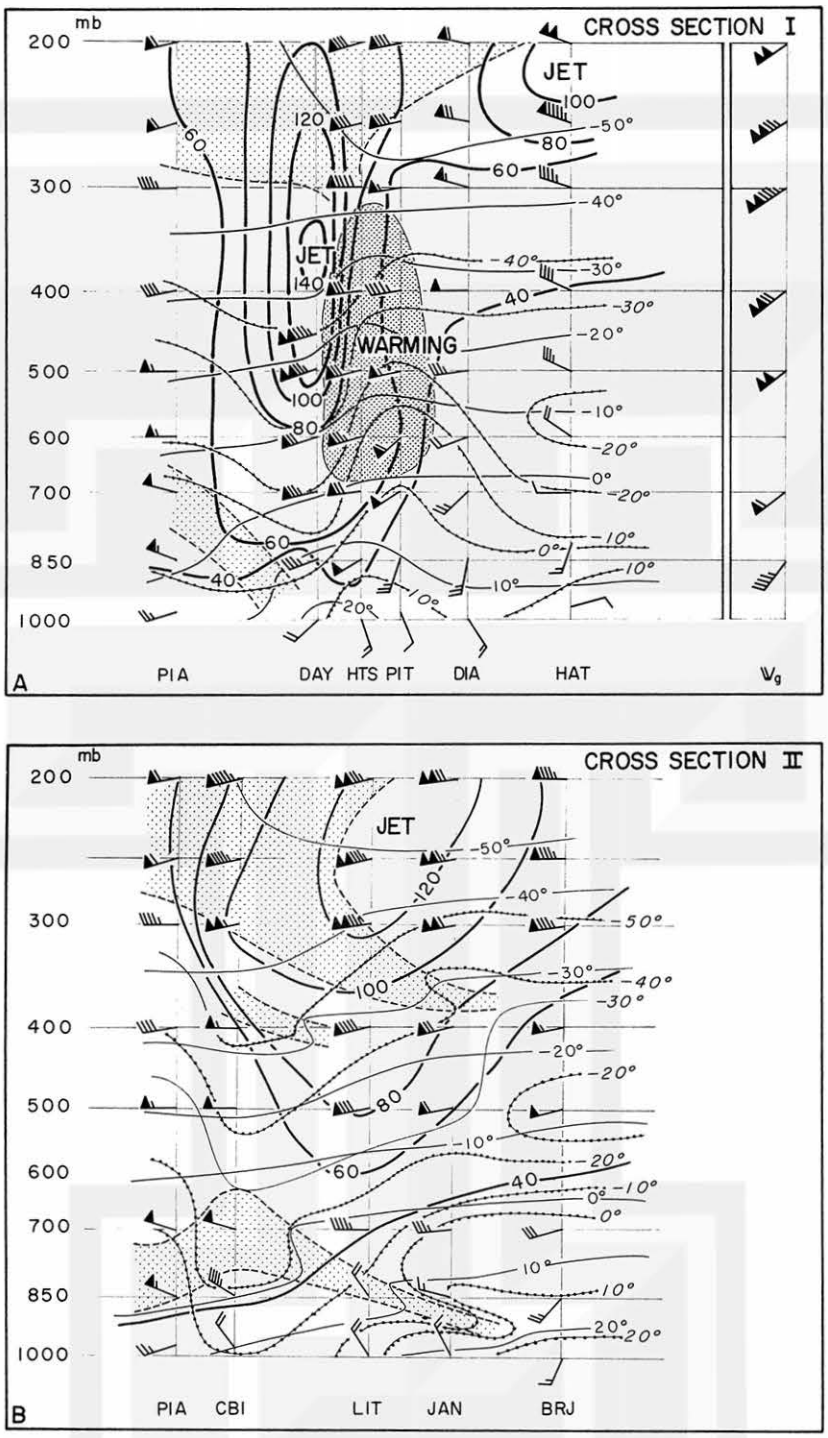

Fig. 14. The vertical cross section normal to the jet stream. Isotaches, isotherms and isolines of dew-point temperature are indicated by thick, thin and thin-dotted lines, respectively.

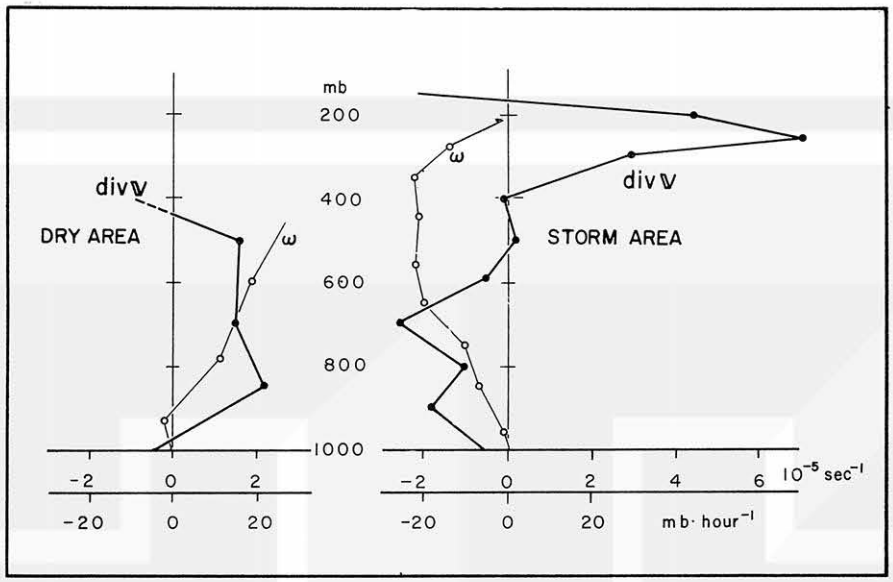

Fig. 15. The vertical distribution of divergence and vertical velocity in the storm area and in the dry area.

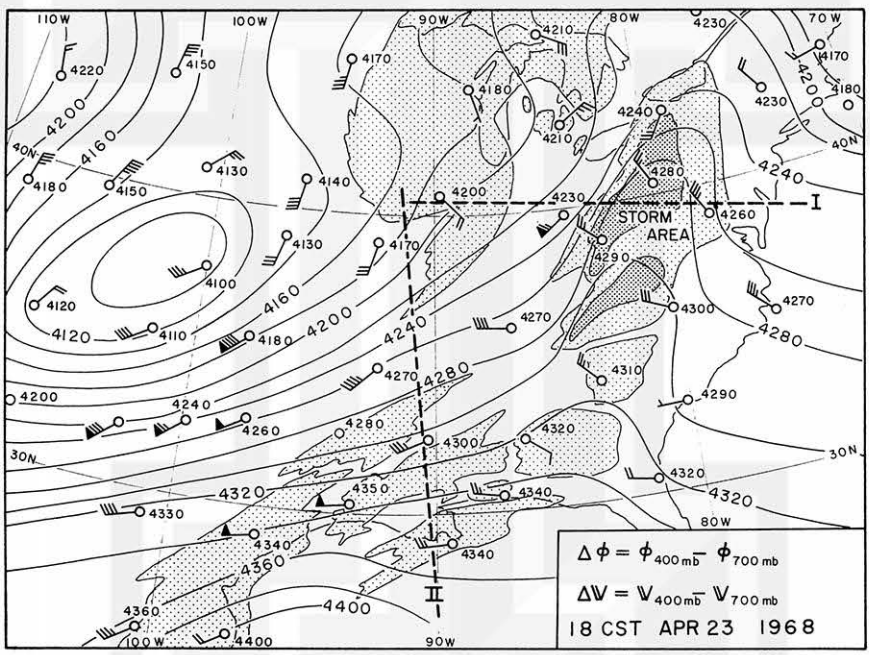

Fig. 16. Thickness of the layer between the 400-mb and 700-mb surface and the difference between the wind velocity at 400-mb and that at 700 mb at 1800 CST. Radar echo and cloud are indicated by dense and thin stippling.

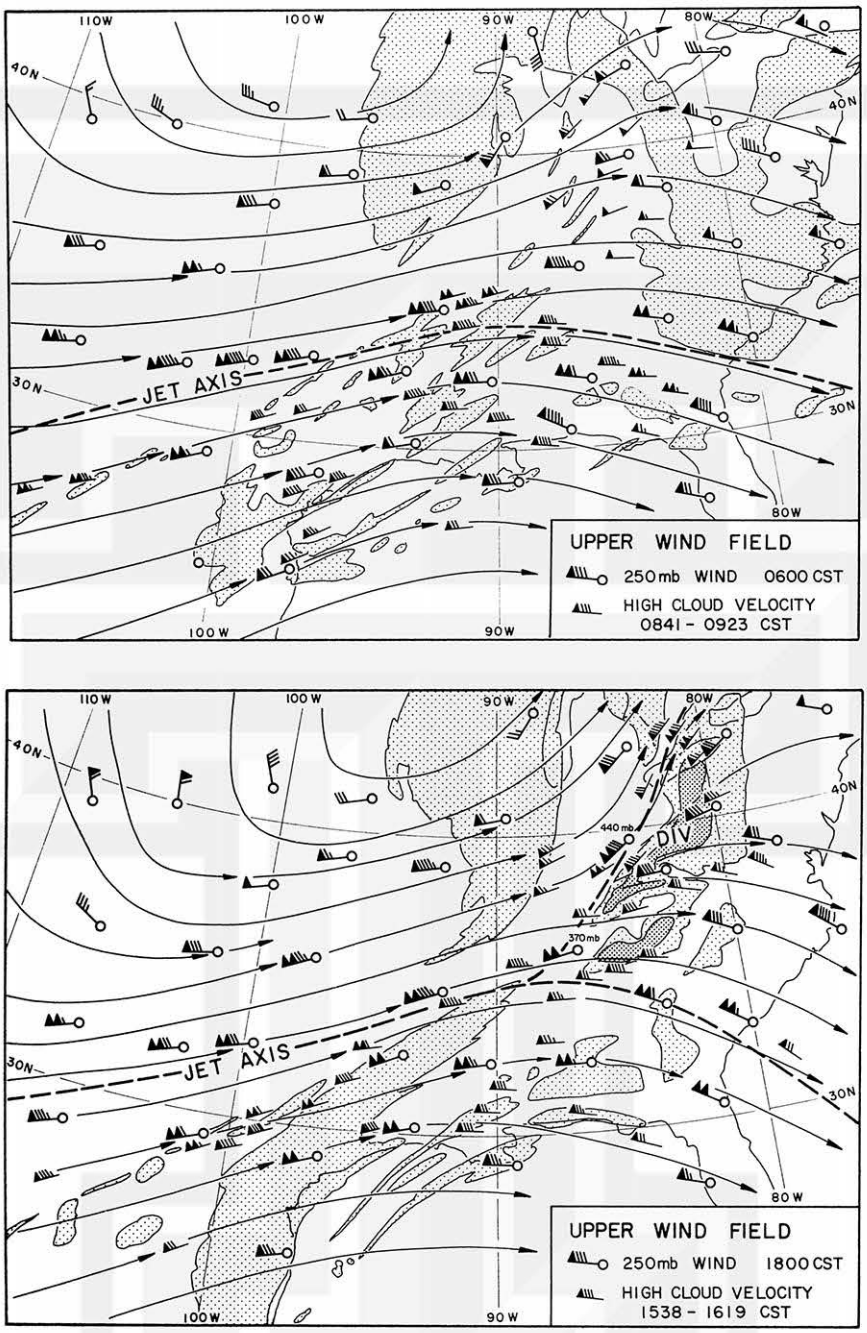

Fig. 17. High-cloud velocity and the 250-mb wind velocity.

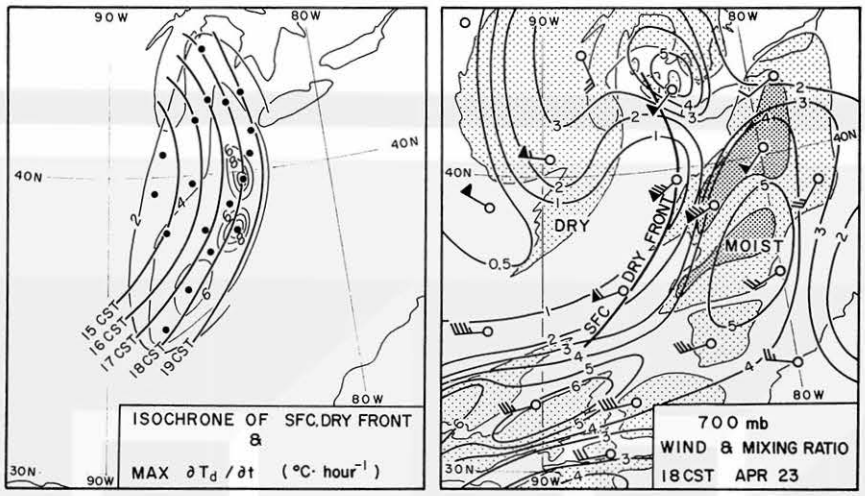

Fig. 18. Left figure: Isochrone of the dry front and maximum decrease of the dewpoint temperature in one hour. Black circles indicate surface observation stations.

Right figure: Mixing ratio and wind at the 700-mb surface.

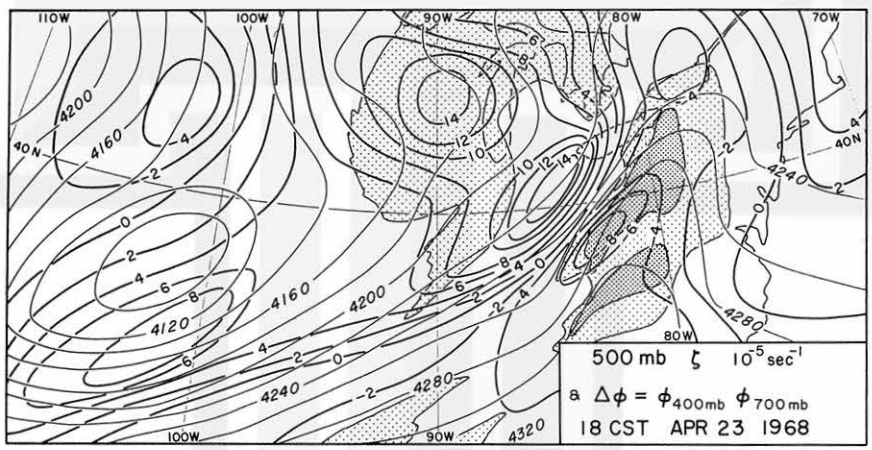

Fig. 19. Relative vorticity at the 500-mb surface and the thickness of the layer between 400 and 700 mb.

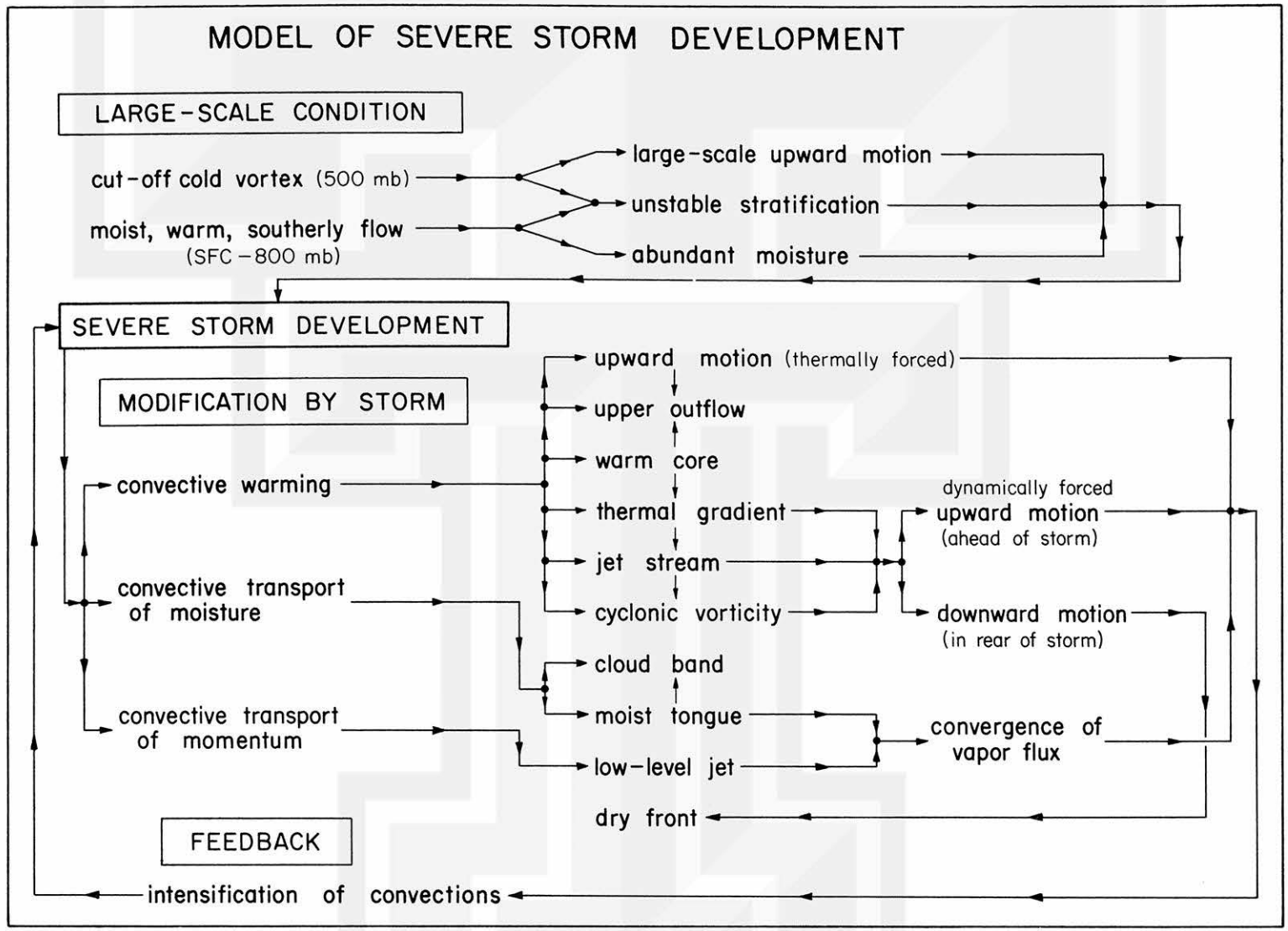

Fig. 20. Schematic model of interaction between the thunderstorms and the large-scale field in the development of storms.

MESOMETEOROLOGY PROJECT - - - RESEARCH PAPERS

(Continued from front cover)

42.* A Study of Factors Contributing to Dissipation of Energy in a Developing Cumulonimbus - Rodger A. Brown and Tetsuya Fujita

43. A Program for Computer Gridding of Satellite Photographs for Mesoscale Research - William D. Bonner

44. Comparison of Grassland Surface Temperatures Measured by TIROS VII and Airborne Radiometers under Clear Sky and Cirriform Cloud Conditions - Ronald M. Reap

45. Death Valley Temperature Analysis Utilizing Nimbus I Infrared Data and Ground-Based Measurements - Ronald M. Reap and Tetsuya Fujita

46. On the "Thunderstorm-High Controversy" - Rodger A. Brown

47. Application of Precise Fujita Method on Nimbus I Photo Gridding - Lt. Cmd. Ruben Nasta

48. A Proposed Method of Estimating Cloud-top Temperature, Cloud Cover, and Emissivity and Whiteness of Clouds from Short- and Long-wave Radiation Data Obtained by TIROS Scanning Radiometers - T. Fujita and H. Grandoso

49. Aerial Survey of the Palm Sunday Tornadoes of April 11, 1965 - Tetsuya Fujita

50. Early Stage of Tornado Development as Revealed by Satellite Photographs - Tetsuya Fujita

51. Features and Motions of Radar Echoes on Palm Sunday, 1965 - D. L. Bradbury and T. Fujita

52. Stability and Differential Advection Associated with Tornado Development - Tetsuya Fujita and Dorothy L. Bradbury

53. Estimated Wind Speeds of the Palm Sunday Tornadoes - Tetsuya Fujita

54. On the Determination of Exchange Coefficients: Part II - Rotating and Nonrotating Convective Currents - Rodger A. Brown

55. Satellite Meteorological Study of Evaporation and Cloud Formation over the Western Pacific under the Influence of the Winter Monsoon - K. Tsuchiya and T. Fujita

56. A Proposed Mechanism of Snowstorm Mesojet over Japan under the Influence of the Winter Monsoon - T. Fujita and K. Tsuchiya

57. Some Effects of Lake Michigan upon Squall Lines and Summertime Convection - Walter A. Lyons

58. Angular Dependence of Reflection from Stratiform Clouds as Measured by TIROS IV Scanning Radiometers - A. Rabbe

59. Use of Wet-beam Doppler Winds in the Determination of the Vertical Velocity of Raindrops inside Hurricane Rainbands - T. Fujita, P. Black and A. Loesch

60. A Model of Typhoons Accompanied by Inner and Outer Rainbands - Tetsuya Fujita, Tatsuo Izawa., Kazuo Watanabe and Ichiro Imai

61. Three-Dimensional Growth Characteristics of an Orographic Thunderstorm System - Rodger A. Brown

62. Split of a Thunderstorm into Anticyclonic and Cyclonic Storms and their Motion as Determined from Numerical Model Experiments - Tetsuya Fujita and Hector Grandoso

63. Preliminary Investigation of Peripheral Subsidence Associated with Hurricane Outflow - Ronald M. Reap

64. The Time Change of Cloud Features in Hurricane Anna, 1961, from the Easterly Wave Stage to Hurricane Dissipation - James E. Arnold

65. Easterly Wave Activity over Africa and in the Atlantic with a Note on the Intertropical Convergence Zone during Early July 1961 - James E. Arnold

66. Mesoscale Motions in Oceanic Stratus as Revealed by Satellite Data - Walter A. Lyons and Tetsuya Fujita

67. Mesoscale Aspects of Orographic Influences on Flow and Precipitation Patterns - Tetsuya Fujita

68. A Mesometeorological Study of a Subtropical Mesocyclone -Hidetoshi Arakawa, Kazuo Watanabe, Kiyoshi Tsuchiya and Tetsuya Fujita

69. Estimation of Tornado Wind Speed from Characteristic Ground Marks - Tetsuya Fujita, Dorothy L. Bradbury and Peter G. Black

70. Computation of Height and Velocity of Clouds from Dual, Whole-Sky, Time-Lapse Picture Sequences - Dorothy L. Bradbury and Tetsuya Fujita

71. A Study of Mesoscale Cloud Motions Computed from ATS-I and Terrestrial Photographs - Tetsuya Fujita, Dorothy L. Bradbury, Clifford Murino and Louis Hull

72. Aerial Measurement of Radiation Temperatures over Mt. Fuji and Tokyo Areas and Their Application to the Determination of Ground- and Water-Surface Temperatures - Tetsuya Fujita, Gisela Baralt and Kiyoshi Tsuchiya

73. Angular Dependence of Reflected Solar Radiation from Sahara Measured by TIROS VII in a Torquing Maneuver - Rene Mendez.

74. The Control of Summertime Cumuli and Thunderstorms by Lake Michigan During Non-Lake Breeze Conditions - Walter A. Lyons and John W. Wilson

75. Heavy Snow in the Chicago Area as Revealed by Satellite Pictures - James Bunting and Donna Lamb

76. A Model of Typhoons with Outflow and Subsidence Layers - Tatsuo Izawa

* out of print

(continued on outside back cover)

SATELLITE AND MESOMETEOROLOGY RESEARCH PROJECT - - - PAPERS

(Continued from inside back cover)

77. Yaw corrections for Accurate Gridding of Nimbus HRIR Data - Roland A. Madden

78. Formation and Structure of Equatorial Anticyclones Caused by Large-Scale Cross Equatorial Flows Determined by ATS I Photographs - Tetsuya T. Fujita and Kazuo Watanabe and Tatsuo Izawa

79. Determination of Mass Outflow from a Thunderstorm Complex Using ATS III Pictures - T. T. Fujita and D. L. Bradbury

80. Development of a Dry Line as Shown by ATS Cloud Photography and Verified by Radar and Conventional Aerological Data - Dorothy L. Bradbury

81. Dynamical Analysis of Outflow from Tornado-Producing Thunderstorms as Revealed by ATS III Pictures - K. Ninomiya

82. Computation of Cloud Heights from Shadow Positions through Single Image Photogrammetry of Apollo Pictures - T. T. Fujita

83. Aircraft, Spacecraft, Satellite and Radar Observations of Hurricane Gladys, 1968- R. Cecil Gentry, Tetsuya T. Fujita and Robert C. Sheets

84. Basic Problems on Cloud Identification Related to the Design of SMS-GOES Spin Scan Radiometers - Tetsuya Theodore Fujita